The euAP1 Protein MPF3 Represses *MPF2* to Specify Floral Calyx Identity and Displays Crucial Roles in Chinese Lantern Development in *Physalis*[C][W]

Jing Zhao,[a,b,1] Ying Tian,[a,1] Ji-Si Zhang,[a,b] Man Zhao,[a,b] Pichang Gong,[a,b] Simone Riss,[c,2] Rainer Saedler,[c] and Chaoying He[a,3]

[a] State Key Laboratory of Systematic and Evolutionary Botany, Institute of Botany, Chinese Academy of Sciences, Xiangshan, 100093 Beijing, China
[b] University of Chinese Academy of Sciences, 100049 Beijing, China
[c] Max-Planck-Institute for Plant Breeding Research, Department of Molecular Plant Genetics, 50829 Cologne, Germany

ORCID IDs: 0000-0001-6984-228X (J.Z.); 0000-0002-2550-0170 (C.H.).

The Chinese lantern phenotype or inflated calyx syndrome (ICS) is a postfloral morphological novelty in *Physalis*. Its origin is associated with the heterotopic expression of the MADS box gene 2 from *Physalis floridana* (*MPF2*) in floral organs, yet the process underlying its identity remains elusive. Here, we show that *MPF3*, which is expressed specifically in floral tissues, encodes a core eudicot APETALA1-like (euAP1) MADS-domain protein. MPF3 was primarily localized to the nucleus, and it interacted with MPF2 and some floral MADS-domain proteins to selectively bind the CC-A-rich-GG (CArG) boxes in the *MPF2* promoter. Downregulating *MPF3* resulted in a dramatic elevation in *MPF2* in the calyces and androecium, leading to enlarged and leaf-like floral calyces; however, the postfloral lantern was smaller and deformed. Starch accumulation in pollen was blocked. *MPF3 MPF2* double knockdowns showed normal floral calyces and more mature pollen than those found in plants in which either *MPF3* or *MPF2* was downregulated. Therefore, MPF3 specifies calyx identity and regulates ICS formation and male fertility through interactions with *MPF2*/MPF2. Furthermore, both genes were found to activate *Physalis floridana* invertase gene 4 homolog, which encodes an invertase cleaving Suc, a putative key gene in sugar partitioning. The novel role of the MPF3-*MPF2* regulatory circuit in male fertility is integral to the origin of ICS. Our results shed light on the evolution and development of ICS in *Physalis* and on the functional evolution of *euAP1*s in angiosperms.

INTRODUCTION

MADS box genes, as core transcriptional regulators, are associated with the evolution and development of the flower (Theissen and Melzer, 2007), which is the central identifying feature of angiosperms. Alterations in either spatial or temporal expression are involved in floral structural diversification and the origin of floral morphological novelties (Kanno et al., 2003; He et al., 2004; He and Saedler, 2005). Within Solanaceae, the genus *Physalis* features the Chinese lantern as a postfloral morphological novelty, while its close relative *Solanum* does not develop any such traits. The lantern is a derivative of the calyx, which inflates to a balloon-like structure encapsulating the berry after fertilization; thus, the Chinese lantern phenotype is also termed inflated calyx syndrome (ICS). Hormonal signals that appear to be released at fertilization trigger calyx inflation (He and Saedler, 2007). Further

molecular genetic analyses revealed that the MADS box gene *MPF2*, an ortholog of *AGAMOUS-LIKE24* (*AGL24*) in *Arabidopsis thaliana*, is heterotopically expressed in floral organs by the alteration of its own promoter, a key step associated with the evolutionary origin of ICS in *Physalis* (He and Saedler, 2005). The integration of MPF2 into floral development partially occurs via protein interactions with other floral MADS-domain proteins, such as MPF3 (encoded by MADS box gene 3 from *Physalis floridana* [*MPF3*]) and PFAG (encoded by the *Arabidopsis* AGAMOUS ortholog from *P. floridana* [*PFAG*]) (He et al., 2007). *MPF2*-specific downregulation via RNA interference (RNAi) revealed that MPF2 has two functions during floral development of *Physalis*: (1) expression of postfloral calyx inflation by regulating cell division and cell expansion and (2) regulation of male fertility (pollen development). Since unsuccessful fertilization usually leads to the abolition of ICS development, male fertility appears to be integral to the origin of ICS (He and Saedler, 2005). ICS is hypothesized to be the result of postfloral calyx inflation. However, the processes underlying the identity of the floral calyx and postfloral ICS are not yet understood.

These processes have been elucidated by investigations using model plant systems. Genetic analyses of floral mutants in *Arabidopsis* identified the underlying genetic regulation of floral organ identity as formulated in the ABC model (Schwarz-Sommer et al., 1990; Coen and Meyerowitz, 1991; Weigel and Meyerowitz, 1994): A-function alone specifies sepal identity; A- and B-functions together control petal identity; B- and C-functions together control

stamen identity; and C-function alone specifies carpel identity. The *SEPALLATA* (*SEP*) genes, *SEP1/2/3/4*, termed E-function genes, are also required for the specification of organ identity (Pelaz et al., 2000; Theissen and Saedler, 2001; Ditta et al., 2004). These MADS-domain proteins regulate each other in a reciprocal fashion and form complexes so as to exert their regulatory roles (Honma and Goto, 2001; Ng and Yanofsky, 2001; Theissen and Saedler, 2001; Theissen and Melzer, 2007; Gregis et al., 2009). The first and only identified A-function MADS box gene is *APE-TALA1* (*AP1*) in *Arabidopsis* (Mandel et al., 1992); however, the concept of A-function was challenged by the role of *SQUAMOSA* (*SQUA*) in *Antirrhinum majus*, which does not determine the sepal and petal organ identity (Schwarz-Sommer et al., 1990; Huijser et al., 1992). Accumulated evidence now shows that the A-function is not conserved in eudicots (Litt and Kramer, 2010), but that several *AP1/SQUA* homologs are involved in determining sepal identity within the core eudicots (Berbel et al., 2001; Taylor et al., 2002; Vrebalov et al., 2002; Benlloch et al., 2006). Furthermore, this function requires participation of other genes. In *Arabidopsis*, sepal organ identity has been well documented as being regulated by *AP1*, *AGL24*, and *SEP* (Mandel et al., 1992; Bowman et al., 1993; Ditta et al., 2004; Yu et al., 2004). In addition, the direct repression of *AGL24* by AP1 is a crucial step in flower development (Yu et al., 2004). Thus, both *AGL24* overexpressors and *ap1* mutants feature an identical phenotypic variation with leaf-like sepals and indeterminate inflorescences (He et al., 2004; Yu et al., 2004). *AGL24* in *Arabidopsis* is the ortholog of *MPF2* in *Physalis* and of *Solanum tuberosum* MADS-box gene 16 (*STMADS16*) in *Solanum* (He and Saedler, 2005). Unlike *STMADS16*, *MPF2* mRNA is heterotopically expressed in floral organs (~10 to 20% of the leaf level). Heterotopic expression is crucial to the origin of ICS in *Physalis* (He and Saedler, 2005) and a hallmark for plants of Solanaceae family that feature ICS (Hu and Saedler, 2007). Further overexpression of either *MPF2* or *STMADS16* can lead to leaf-like sepals in transgenic *Solanum* plants (He and Saedler, 2007). Similarly, an AP1/SQUA-like transcription factor is assumed to repress *STMADS16* or *MPF2* in floral organs. As observed in *Solanum*, *STMADS16* was expressed in vegetative tissues only; however, alterations in the *MPF2* promoter itself led to leakage of its expression to floral organs in *Physalis* (He and Saedler, 2005).

Multiple copies of *AP1/SQUA*-like genes are known to have evolved in plant genomes, and they fall into the core eudicot *APETALA1*-like (*euAP1*), core eudicot *FRUITFULL*-like (*euFUL*), and *FRUITFULL*-like (*FL*) subclades (Ferrándiz et al., 2000; Litt and Irish, 2003; Preston and Kellogg, 2006; Litt, 2007; Shan et al., 2007). Only the *euAP1* members have been shown to be involved in specifying sepal identity within the core eudicots (Mandel et al., 1992; Gustafson-Brown et al., 1994; Berbel et al., 2001; Taylor et al., 2002; Vrebalov et al., 2002; Benlloch et al., 2006). Since in *Solanum*, Le-MADS-MC regulates sepal organ identity (Vrebalov et al., 2002), we assumed that its putative ortholog MPF3 in *Physalis* described by He et al. (2004) might also specify calyx identity. MPF2 was shown to interact with MPF3 in yeast (He et al., 2007); therefore, we hypothesized that MPF3 interacts with *MPF2*/MPF2 genetically and physically to specify calyx identity and regulate ICS development. We conducted this study with three main objectives: namely, to determine

(1) whether a regulatory circuit exists in *Physalis* to control floral calyx identity; (2) whether the postfloral calyx inflation, driven by the heterotopic expression of *MPF2*, results from the alteration of floral calyx identity; and (3) the role of MPF3 in the development of ICS.

We isolated four *AP1/SQUA*-like genes from *Physalis*. Phylogenetic and microsynteny analyses demonstrated that *MPF3* is one of the *euAP1* members that shares a similar expression pattern in floral development. Using two RNA silencing approaches, RNAi and virus-induced gene silencing (VIGS), we discovered the role of MPF3 in determining calyx identity and the size of the Chinese lantern structure. In addition, we showed that MPF3 plays a vital role in male fertility. These findings are supported by observations regarding MPF3, including its mRNA accumulation pattern, interacting protein spectrum, and its genetic regulation of *MPF2*. *PFINV4* is a putative ortholog of *INV4*, which encodes an invertase that cleaves Suc, and is the key gene that regulates pollen maturation in rice (*Oryza sativa*) and lily (*Lilium longiflorum*) (Ranwala and Miller, 1998; Oliver et al., 2005). Genetic regulation of *PFINV4* by MPF3 indicates a novel way for MADS box transcription factors to influence the development of male fertility. We showed that the development of ICS after fertilization in *Physalis* was not a result of altered floral calyx organ identity. Furthermore, we discuss neofunctionalization or functional diversification that accompanies the evolution of novel genetic and physical interactions within *euAP1* genes of angiosperms.

RESULTS

Molecular Characterization of *AP1/SQUA*-Like Genes from *Physalis*

Multiple copies of *AP1/SQUA*-like genes exist in the genomes of all angiosperm species examined, and they share high sequence identities (Litt and Irish, 2003; Preston and Kellogg, 2006; Litt, 2007; Shan et al., 2007). An *AP1/SQUA*-like cDNA, named *MPF3*, was previously isolated from *P. floridana* (He et al., 2004). We performed a DNA gel blot analysis using an *MPF3* cDNA fragment encoding the IKC domain as a probe to estimate the copy numbers of *MPF3*-like genes in *P. floridana*. The results suggest that four copies may exist in the genome of *P. floridana* (Figure 1A). In line with this, we obtained four *AP1/SQUA*-like cDNAs. Bayesian and maximum likelihood phylogenetic trees were reconstructed to show that the four genes belong to three subclades, and these genes were named *MPF3* (*euAP1*), *PFFUL1*, *PFFUL2* (*euFUL*), and *PFFL* (*FL*) (see Supplemental Figure 1 and Supplemental Data Set 1 online). Since the coding region of these paralogs had changed to the extent that the four copies were evolutionarily distinct, their expression patterns also might have become more diversified.

The mRNA expression patterns of *AP1/SQUA*-like genes in *P. floridana* were therefore measured using real-time RT-PCR. Total RNA was extracted from leaves, pedicels, flower buds, and the four whorls of mature flowers. As shown in Figure 1B, among these *AP1/SQUA*-like paralogs (*MPF3*, *PFFUL1/2*, and *PFFL*), only *MPF3* was found not to be expressed in vegetative organs
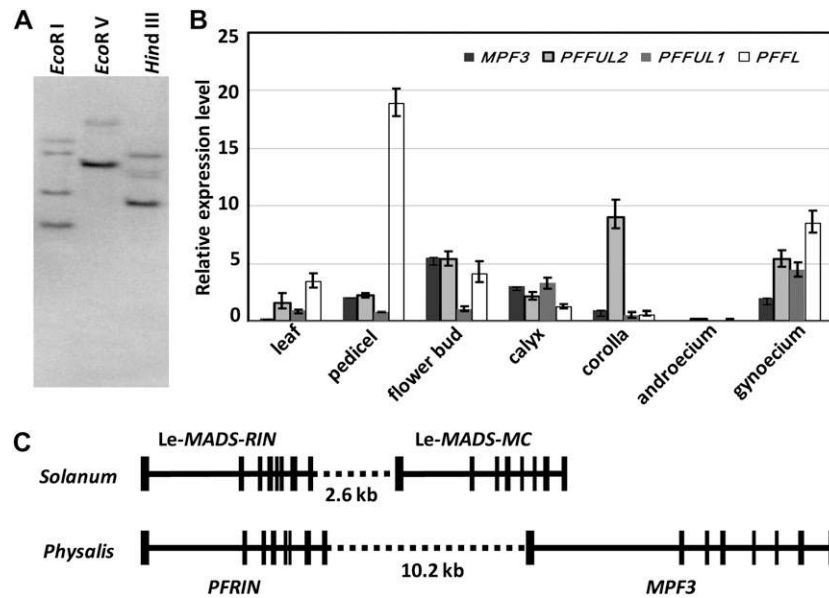
Figure 1. Characterization of *AP1/SQUA*-Like Genes in *Physalis*.

(A) DNA gel blotting using the *MPF3*-specific cDNA fragment as a probe. Genomic DNA was digested using the restriction enzymes indicated.
(B) Expression of *AP1/SQUA*-like genes. For each sample, the genes from left to right are *MPF3*, *PFFUL2*, *PFFUL1*, and *PFFL*. *Actin* was used as an internal control. Experiments were performed on three independent biological samples. The average expression level and sd are presented.
(C) Local microsynteny of *MPF3* and its ortholog Le-*MADS-MC*. Vertical lines indicate exons, and horizontal lines indicate promoter, intron, and intergenic sequences.

(leaves). Their transcripts were detected at different levels, predominantly in flower buds, pedicels, calyces, corolla, and gynoecia, of mature flowers. All transcripts were expressed in the androecium at extremely low levels or not at all. Consistent with the diverse expression patterns of *AP1/SQUA*-like genes (Litt, 2007), the four paralogs in *P. floridana* also evolved distinct expression patterns after duplication.

Local Synteny Provides Further Support That *MPF3* Is an Ortholog of Le-*MADS-MC*

The phylogeny and expression analyses suggest that *MPF3*, as a *euAP1*, is a putative ortholog of Le-*MADS-MC*. However, additional evidence for its orthology comes from microsynteny analysis. In tomato (*Solanum lycopersicum*), Le-*MADS-MC* is physically linked to another MADS box gene, Le-*MADS-RIN*, in the genome (Vrebalov et al., 2002). If *MPF3* is the true ortholog of Le-*MADS-MC*, *MPF3* would also be linked to the *Physalis* ortholog of Le-*MADS-RIN*. In the *Physalis* floral transcriptome, the putative ortholog of Le-*MADS-RIN* was found and named *PFRIN* (Unigene119993_P106; see Supplemental Data Set 2 online), and the two shared 86.4% amino acid sequence identity. Next, we analyzed the linkage of *MPF3* and *PFRIN* using the long-template PCR approach. First, we retrieved a 9763-bp fragment harboring the *MPF3* locus and a 5725-bp fragment harboring the *PFRIN* locus. Both gene pairs share a conserved intron-exon structure between *Solanum* and *Physalis* (Figure 1C). We then amplified the linkage region (~10.2 kb) between *MPF3* and *PFRIN*. Overall, we constructed a 25.69-kb DNA fragment

from the *Physalis* genome (Figure 1C). These data indicate that local microsynteny has been well maintained between the two genomes during evolution, which further substantiates the orthology of *MPF3* and Le-*MADS-MC*, which share 91.5% amino acid sequence identity, suggesting that the role of MPF3 in flowers might be similar to that of Le-MADS-MC.

To elucidate the function of MPF3, we characterized the fine floral expression of the gene, the subcellular localization of the protein, and the interacting proteins in *Physalis*.

Fine Floral Expression Pattern of *MPF3* in *Physalis*

Real-time RT-PCR showed that *MPF3* expression was restricted to floral organs (Figure 1B). To characterize *MPF3* expression during floral development, we performed RNA gel blotting and mRNA in situ hybridization. To avoid possible cross-hybridization with other paralogs, a fragment spanning the most variable C-domain and the 3′-untranslated region of *MPF3* was used as a *MPF3*-specific probe. Using mRNA in situ hybridization (Figure 2A), *MPF3* transcripts were detected throughout the floral meristem. During floral organ initiation, *MPF3* was found to be expressed in the primordia of the two outer whorls (calyx and corolla) and in the inner whorls (androecium and gynoecium). At the completion of flower bud formation, *MPF3* expression was mainly observed in the outer whorl regions. The expression signal was also detected in vascular tissues of the pedicel during flower formation. These findings suggest that MPF3 may initiate floral meristems and specify floral organ identity. RNA gel blots showed that *MPF3* mRNA was abundant in the calyx, corolla, and
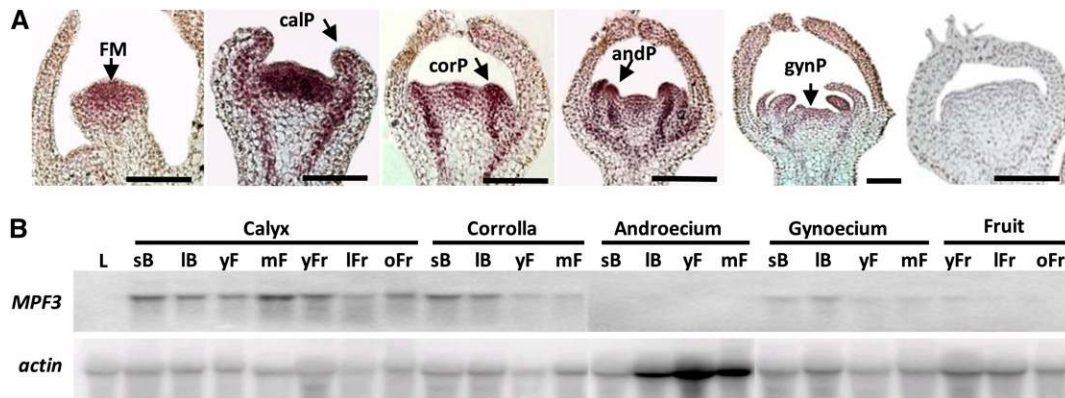
Figure 2. Expression of *MPF3* during Flower Development in *Physalis*.

(A) *MPF3* mRNA in situ hybridization in early floral development. The floral meristem (FM), primordia of calyx (calP), corolla (corP), androecium (andP), and gynoecium (gynP) are indicated by arrows. From left to right, *MPF3*-antisense was probed in the first five images, and *MPF3*-sense was probed in the last image. Bars = 50 μm.

(B) RNA gel blot analysis of *MPF3* after flower formation. Total RNAs were isolated from the leaf (L), calyx, corolla, androecium, gynoecium, and fruit. The developmental stages were roughly determined as small buds (sB), large buds (lB), young flowers (yF), mature flowers (mF), young fruits (yFr), large fruits (lFr), and old fruits (oFr). *Actin* was reprobed after stripping off *MPF3* and was used as a loading control.

gynoecium from the time that floral buds appeared to anthesis, while no expression was detected in the androecium (Figure 2B). After fertilization, *MPF3* was also detectable in developing fruits, albeit at a relatively low level. Consistent with the results obtained from real-time RT-PCR (Figure 1B), no *MPF3* mRNA was detected in leaves (Figure 2B), thereby verifying the specificity of the *MPF3* probe. This expression pattern strongly suggests a role for MPF3 throughout floral development, including the initiation of floral meristems, specification of floral organ identity, and growth of floral and postfloral organs.

MPF3 Is Primarily Localized to the Nucleus

In addition to mRNA accumulation and distribution, the localization of a protein is another important aspect of gene activity. The precise subcellular localization of MPF3 would indicate whether or not this protein acts as a transcription factor. To test this, we linked the completed MPF3 open reading frame (ORF) with *GFP* (for green fluorescent protein) and infiltrated this construct via *Agrobacterium tumefaciens* into plant cells to synthesize a MPF3-GFP fusion protein. Cells transfected with GFP alone were used as a control. In our analyses, the GFP signal was detected in whole cells in both the MPF3-GFP fusion protein and control (Figures 3A and 3B). However, for the MPF3 fusion protein, the signal was primarily detected in the nucleus and only slightly in the cytoplasm (Figure 3A). We verified this by quantifying the relative GFP fluorescence intensity. In comparison to the GFP control, the nuclear-to-cytoplasmic ratio of the GFP signal in cells harboring the MPF3-GFP fusion increased significantly (P = 2.45 × 10^{-21}; Figure 3B), indicating that, after translation, MPF3 was primarily transported to the nucleus. This localization suggests that MPF3, alone or via an interaction with other proteins, has a regulatory role in the nucleus.

Characterization of MPF3′ MADS-Domain Interacting Proteins

MADS-domain proteins often form dimers and complexes that regulate transcription (Davies et al., 1996; Egea-Cortines et al., 1999; Honma and Goto, 2001). To identify which other MADS-domain proteins interact with MPF3, yeast two-hybrid analysis was performed. The *Physalis* expression library (He et al., 2007) was directly screened using MPF3 as bait, since it did not self-activate in yeast. Besides MPF2 (He et al., 2007), MPF3 was observed to interact with a series of floral MADS-domain proteins, including PFGLO1, PFGLO2, PFSEP2, PFSEP3, and PFAG (Figure 3C). PFGLO1 and PFGLO2 are homologous to GLOBOSA (GLO) (Tröbner et al., 1992); thus, they might serve as B-function MADS-domain proteins. PFSEP2 and PFSEP3 are E-function proteins and PFAG is a C-function protein (He et al., 2007). We verified the specific interactions between MPF3 (a euAP1 protein) and PFGLO1/2 (B-function proteins) using pull-down assays. Our results suggest that both PFGLO1 and PFGLO2 bind to MPF3 (Figure 3D), thus confirming the observations made in the yeast two-hybrid assays.

To verify these interactions in plant cells, bimolecular fluorescence complementation (BiFC) analyses using yellow fluorescent protein (YFP)-split technology were performed. The N-terminal (YFPn) and C-terminal (YFPc) halves of YFP were fused in frame to the C termini of the proteins examined, and all combinations of the two fusion proteins with either YFPn or YFPc were coexpressed in plant cells to assess whether or not they underwent heterodimerization. The YFPn and YFPc halves without the MADS-domain protein fusion were coexpressed as a negative control. Coexpression of MPF3-YFPn with MPF2-YFPc and with PFAG-YFPc yielded clear YFP signals exclusively in the nucleus (Figures 3F and 3H). This confirmed that MPF3 stably interacted with MPF2 and PFAG in the nucleus. Surprisingly, no visible YFP signal was detected using any combinations
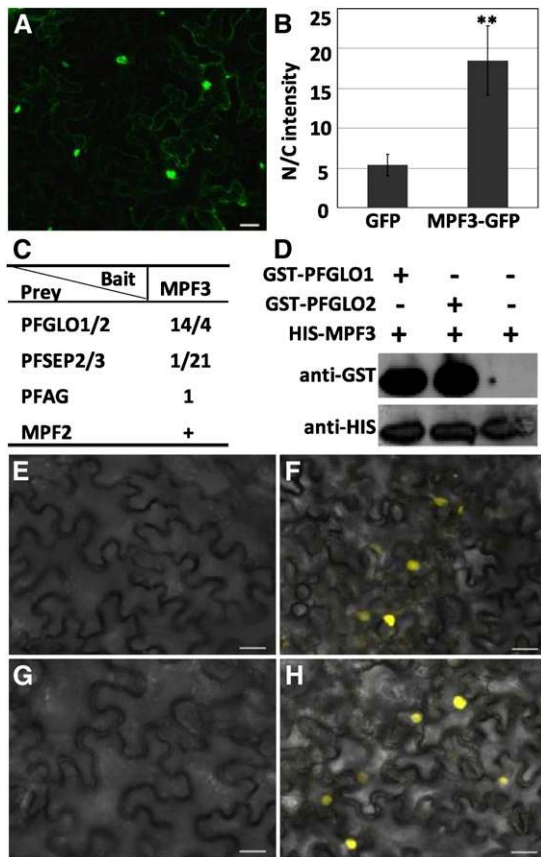
Figure 3. Subcellular Localization of MPF3 and Its Interacting Proteins.

(A) Subcellular localization of MPF3.

(B) The relative proportional fluorescence of the nucleus to the cytoplasm (N/C) between the GFP control and MPF3-GFP fusion. Thirty-two cells were analyzed in the GFP control and 20 in the MPF3-GFP fusion. The mean and SD are presented. Asterisks designate significance relative to the control (two-tailed Student's *t* test, $P = 2.45 \times 10^{-21}$).

(C) Results of library screen using MPF3 as bait. The number stands for the independent colony that was obtained and sequenced. The previous observation of MPF3 interacting with MPF2 (He et al., 2007) is included and indicated by a plus symbol.

(D) Pull-down assay to confirm that MPF3 interacts with PFGLO1/2. The first two lanes are the results of heterodimer formation of the two proteins as indicated (see Methods). The last lane denotes His-MPF3 proteins loaded as control. Plus and minus symbols stand for inclusion or exclusion of the corresponding proteins, respectively.

(E) to **(H)** Results of BiFC analyses. The YFPn and YFPc empty vectors were coexpressed as a negative control **(E)**. MPF3-MPF2 **(F)**, MPF3-PFGLO1 **(G)**, and MPF3-PFAG **(H)**. A YFP signal suggests that the corresponding interaction occurs. As in **(G)**, no YFP signal was detected in MPF3-PFGLO2. The results (**[F]** to **[H]**) are from the combination of MPF3-YFPn, and the indicated proteins were fused with YFPc at their C termini. Bars = 20 μm.

of MPF3 and PFGLO1/2 fusion protein with either YFPn or YFPc (Figure 3G). As expected, no signal was observed in the control (Figure 3E). The failure to detect YFP signals in the MPF3 and PFGLO1/2 interactions suggests that these interactions are weak or unstable in plant leaf cells. Accordingly, we quantified their

interacting strengths in yeast and found that MPF3 interacted less strongly with PFGLO1 and PFGLO2 than with MPF2 and PFSEP3, as revealed by relatively low β-galactosidase activity (see Supplemental Figure 2A online). Nonetheless, MPF3 and PFAG had equivalent weak interacting strengths. In addition, all of these proteins formed homodimers (see Supplemental Figure 2B online).

The stable and transient interactions of MPF3 with these floral MADS-domain transcription factors further support the possibility that these proteins have roles in floral pathways in *Physalis*.

Transgenic Analyses Reveal Crucial Roles for *MPF3* in Floral Development

As there are currently no *mpf3* mutants available, we inferred the role of *MPF3* using reverse genetic approaches in *Physalis*. Overexpression and RNAi strategies were used to infer the roles of *MPF3* in *P. floridana*. Three *MPF3* overexpression lines (OE1, OE2, and OE3) were generated (see Supplemental Table 1 online). Overexpression of *MPF3* did not promote any visible morphological variations compared with wild-type *Physalis*. However, the timing of the floral phase transition was found to be altered. Wild-type *Physalis* flowered ~30 d after germination, when the node number reached 8 to 9 in a growth chamber under long-day conditions, while the transgenic plants flowered ~28 d after germination, with approximately six nodes under the same conditions (see Supplemental Table 1 online). This result deviated significantly from the wild type ($P < 4.2 \times 10^{-5}$ for the time of first flower opening and $P < 1.59 \times 10^{-10}$ for node number at flowering time), suggesting that *MPF3* promoted flowering in *Physalis*.

Six independent lines (R1, R3, R5, R7, R8, and R14) of *MPF3*-RNAi transgenic *Physalis* plants were generated and analyzed. Real-time RT-PCR analyses indicated that *MPF3* mRNA was reduced by 60 to 90% in comparison to the wild type, while the other three homologs were not downregulated; yet, the level of *PFFL* mRNA appeared to be slightly elevated, indicating that *MPF3* was specifically knocked down in these transgenic lines (Figure 4A). The phase transition of the transgenic plants was not affected (see Supplemental Table 1 online). In comparison with the wild type (Figure 4B), the solitary flowers with elongated pedicels were uniformly seen (Figure 4C), suggesting that floral meristem identity was not affected by the downregulation of *MPF3*. Nevertheless, dramatic floral phenotypic variations were observed (e.g., the morphology of the floral calyx was affected).

Compared with the calyces of the wild type (Figures 4B and 4D), leaf-like calyces were observed throughout the entire spectrum from young flower buds to mature flowers in the *MPF3*-RNAi transgenic *Physalis* lines (i.e., R3; Figures 4C and 4E). The epidermal cells of the floral calyx were subjected to scanning electron microscopy analysis. Prior to anthesis, the calyx cells of wild-type *Physalis* were usually small and undifferentiated (Figure 4G; Hu and Saedler, 2007). The cells were enlarged, and cellular morphology was transformed into shape typical of leaf cells (strongly lobate) in the floral calyx of *MPF3*-RNAi mutants (Figure 4H), resembling leaf cells (Figure 4F). Therefore, knocking down of *MPF3* caused a homeotic transformation of the floral calyx into a leaf-like structure by altering cell identity, and this was accompanied by a significant increase in cell size ($P = 4.26 \times 10^{-10}$; Figure 4M). As a result, a significant enlargement
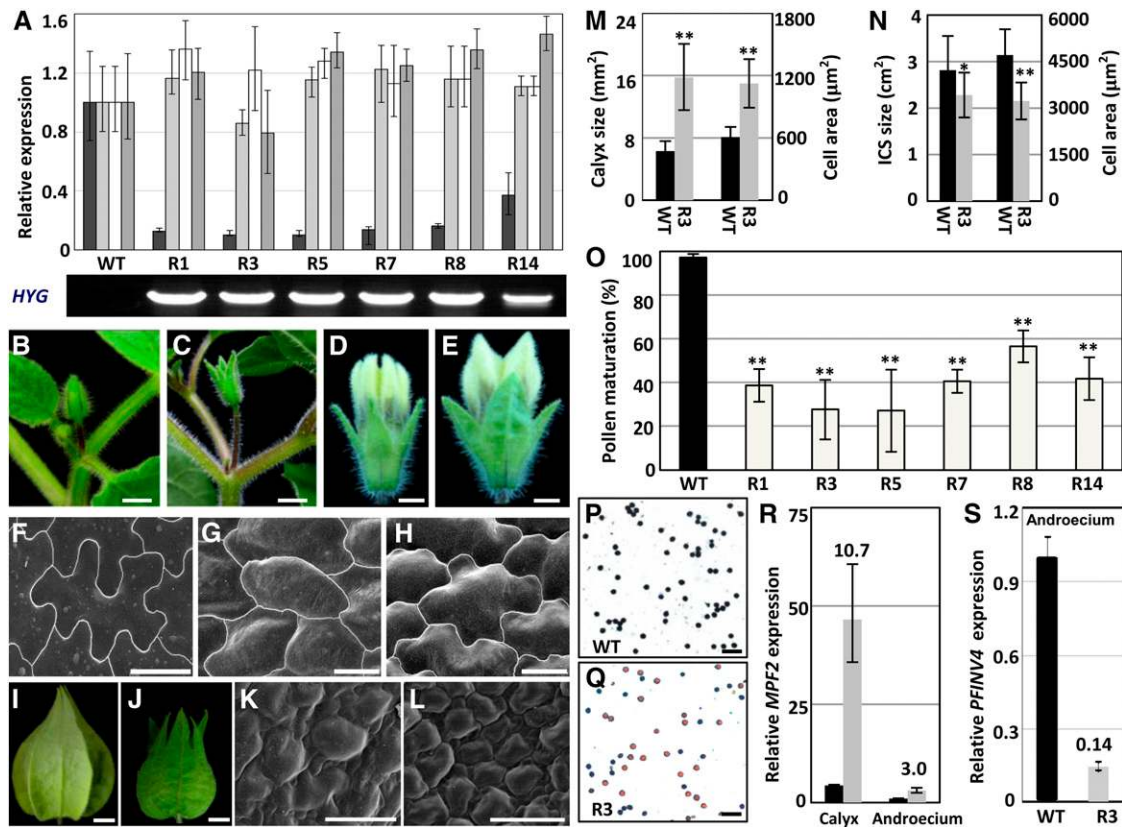
Figure 4. Generation and Analyses of 35S:*MPF3-RNAi* Transgenic *Physalis* Plants.

(A) Genotyping analysis of *35S:MPF3*-RNAi lines. The expression of *MPF3* and its paralogs (*PFFUL1/2* and *PFFL*) were compared between *35S:MPF3*-RNAi lines (R1, R3, R5, R7, R8, and R14) and wild-type (WT) *Physalis* via real-time RT-PCR analysis. Expression of the genetic resistance to hygromycin (*HYG*) was monitored to confirm the identity of transgenic lines. *Actin* gene was used as an internal control. The experiments were repeated using three independent biological samples. Mean expression and SD are presented.

(B) and **(C)** Flower buds of the wild type **(B)** and R3 *35S:MPF3*-RNAi transgenic line **(C)**. Bars = 5 mm.

(D) and **(E)** Floral calyx of the wild type **(D)** and R3 *35S:MPF3*-RNAi transgenic line **(E)**. Bars = 1 mm.

(F) Epidermal cells of the leaf. Bar = 20 μm.

(G) and **(H)** Calyx epidermal cells of the wild type **(G)** and line R3 **(H)**. Bars = 20 μm.

(I) and **(J)** Mature ICS of the wild type **(I)** and line R3 **(J)**. Bar = 5 mm.

(K) and **(L)** Epidermal cells of the ICS from the wild type **(K)** and line R3 **(L)**. Bars = 20 μm.

(M) Size of the calyx surface and epidermal cells of the floral calyx in the wild type and line R3. The number of cells analyzed was 20 and 18 in the wild type and R3, respectively. The number of calyces analyzed was 50 and 25 in the wild type and R3, respectively. Error bar is SD.

(N) Surface area of the ICS and its epidermal cell size in the wild type and line R3. The number of cells analyzed was 20 for both the wild type and R3. The number of calyces analyzed was 46 and 60 in the wild type and R3, respectively. Error bar is SD.

(O) Reduction of pollen maturation of *35S:MPF3*-RNAi transgenic lines. For each line, 10 flowers were evaluated. The mean and SD are presented.

(P) and **(Q)** I$_2$-KI stained pollen from the wild type **(P)** and *35S:MPF3*-RNAi transgenic line R3 **(Q)**. Active pollen is blue, and sterile pollen is tawny. Bars = 100 μm.

(R) and **(S)** Expression of *MPF2* in the calyx and androecium was elevated in the *MPF3*-RNAi line **(R)**, and the expression of *PFINV4* in the androecium was repressed in the *MPF3*-RNAi line **(S)**. Expression of these genes in *35S:MPF3*-RNAi-R3 (gray column) was compared with those in the wild type (black column). The gene expression in the androecium of the wild type was taken as 1, and *Actin* was used as an internal control. The experiments were repeated using three independent biological samples. Mean expression and SD are presented.

of the floral calyx (about twice the size of the wild-type calyx, P = 1.63 × 10^{-14}) was seen in mature flowers (Figures 4E and 4M). However, the final size of the transformed ICS was significantly (P = 0.04) reduced and the morphology deviated from the wild-type ICS (Figures 4I, 4J, and 4N). Surprisingly, in comparison with the wild-type ICS (Figures 4K and 4N), the cell size was significantly (P = 1.32 × 10^{-7}) reduced in the deformed ICS of

MPF3-RNAi line R3 (Figures 4L and 4N). In both developmental stages, variation in cell size could not completely account for the variation in organ size (see Supplemental Table 2 online), suggesting that cell number also increased. These findings indicate that MPF3 regulates cell identity and, thus, the calyx identity prior to anthesis. Moreover, the manner in which MPF3 modulates cell division and expansion was found to be dependent on

the organ contexts. MPF3 is mainly a negative regulator of cell division in both floral and postfloral calyx development. Cell expansion is also negatively regulated in the floral calyx, while it is positively regulated in the fruiting calyx.

The reproductive organs appeared to be normal; however, the fertility of the transgenic plants was poor, as indicated by a low number of berries produced in the absence of artificial pollination. However, pollination with wild-type pollen led to normal fruit development, indicating that the impaired fertility was primarily due to defects in the male organs. Pollen development was first evaluated by iodine-potassium iodide (I_2-KI) staining. Normally, developed pollen stains blue, but we observed that more than 40% of pollen grains did not stain at all in these transgenic plants, a significant deviation from the wild type (P < 2.20×10^{-6}; Figure 4O). One representative sample depicts pollen I_2-KI staining of R3 (27.6% ± 13.5%; Figure 4Q) compared with that of the wild type (97.3% ± 2.8%, Figure 4P). In the *MPF3*-RNAi line, the basic structure of the stamen was evaluated further; however, we did not find any abnormality in stamen development (see Supplemental Figure 3 online). Therefore, downregulation of *MPF3* may directly or indirectly affect sugar translocation to the pollen instead of affecting the stamen structure, thus leading to immature pollen grains.

These transgenic analyses suggest that MPF3 is a multifunctional protein in *Physalis*. It may either play a redundant role or a small role in specifying floral meristem identity so as to promote flowering, and it regulates calyx identity and ICS size. Moreover, our findings suggest that MPF3 has acquired a novel role in male fertility. As a transcription factor, MPF3 might repress or activate downstream genes so as to fulfill its biological functions. We studied this by comparing gene expression between wild-type and *MPF3*-knockdown lines.

Dramatic Repression of *MPF2* and Marked Activation of *PFINV4* by MPF3

MPF2 encodes the key regulator of ICS and male fertility. Knockdown of *MPF2* leads to a small ICS (in extreme cases no ICS develops) and lower pollen yields (He and Saedler, 2005), and overexpression of *MPF2* causes leaf-like sepals in transgenic *Solanum* (He and Saedler, 2007). These aspects were also affected in *MPF3* knockdown lines. Therefore, the expression of *MPF2* was first investigated in the *35S:MPF3*-RNAi transgenic plants. The calyx and androecium of mature flowers were collected, and the RNA was subjected to real-time RT-PCR. *MPF2* mRNA accumulation was elevated ~11-fold in the transformed calyx and threefold in the androecium of R3, in comparison to each respective organ of the wild type (Figure 4R). These data indicate that MPF3, through direct or indirect genetic interaction with *MPF2*, play an important role in the development of the calyx and, subsequently, in male fertility.

To characterize the pollen defect in *MPF3* knockdowns, we also evaluated the genes involved in sugar-partitioning pathways. The Suc transporter genes (*SUT1* and *SUT2*), monosaccharide transporter gene (*MST8*), the carbon starved anther gene (*CSA*) for a MYB domain protein, and the anther cell wall invertase gene (*INV4*) all play essential roles in sugar-partitioning pathways in *Oryza*, *Solanum*, and *Lilium* (Ranwala and Miller, 1998; Leggewie

et al., 2003; Oliver et al., 2005; Büttner, 2007; Zhang et al., 2010). We first searched for closely related homologs in the *Physalis* floral transcriptome (see Supplemental Data Set 2 online) and retrieved *PFSUT1* (Unigene54711_P106), *PFSUT2* (Unigene13767_P106), *PFMST8* (Unigene17675_P106), *PFCSA* (Unigene38938_P106), and *PFINV4* (Unigene70960_P106). These genes are thought to exert similar roles in *Physalis*, since pollen maturation was inhibited in *MPF3* knockdowns. RT-PCR demonstrated that wild-type *PFINV4* was mainly expressed in the androecium and *PFCSA* was specifically expressed in the androecium, while other genes were expressed in both leaves and the androecium (see Supplemental Figure 4 online). Furthermore, we found that *PFINV4* was specifically repressed in the *MPF3*-RNAi lines; however, the other genes were not altered. *INV4*, a key gene regulating sugar partitioning in the Suc sequestration phloem-unloading pathway, encodes an anther-specific invertase for cleaving sucrose (Ranwala and Miller, 1998). Its repression is correlated with Suc accumulation and pollen sterility in rice (Oliver et al., 2005). The expression of *PFINV4* was further monitored in the androecium of the *MPF3*-RNAi line R3. Our results showed that *PFINV4* mRNA accumulation was significantly reduced (to only 14.0% of wild-type levels) in the organs of R3 (Figure 4S). These data suggest that MPF3 regulates pollen maturation, either directly or indirectly, by activating *PFINV4*, and this may regulate sugar partitioning in *Physalis*.

Knockdown of *MPF3* via a VIGS Approach

There was pronounced transgene silencing in the case of *35S:MPF3*-RNAi. In the T3 generation, the effect of *MPF3* silencing was completely ablated. Generation of new double-gene RNAi plants was not feasible, since the procedure is time-consuming. To unravel the role of MPF3 in flower development through genetic interaction with *MPF2*, which is a key regulator of ICS development and pollen maturation (He and Saedler, 2005), we exploited the VIGS approach. The *MPF3*-specific fragment used in our RNAi analysis was introduced into the tobacco rattle virus (TRV) system (Liu et al., 2002) to generate a *MPF3*-VIGS construct. Infection of *Physalis* seedlings resulted in *MPF3* downregulated mutated flowers whose phenotypic variation resembled that of the *35S:MPF3*-RNAi lines. In comparison with the wild type (see Supplemental Figures 5A to 5C online), the floral calyx became leaf like, a smaller deformed ICS developed, and the pedicel was elongated (see Supplemental Figures 5D to 5F online). These alterations in flower morphology and size phenocopied those observed in *35S:MPF3*-RNAi transgenic plants, suggesting that TRV-mediated VIGS is applicable for gene silencing in *Physalis*. Total mRNA from three flowers with dramatic phenotypic deviation from the wild type was subjected to real-time RT-PCR. Although an elevation in *PFFL* was observed (similar to that in *MPF3*-RNAi lines), transcript abundance of *MPF3* in these mutated flowers was efficiently knocked down, and the lowest residual level was 4.1% that of the wild type (see Supplemental Figure 5G online), corroborating the observed phenotypic variations. In these *MPF3*-VIGS flowers, the expression of *MPF2* in the calyx and androecium was significantly increased, particularly in the calyx (44 times that of the wild type; see Supplemental Figure 5H online). *PFINV4* expression in the androecium was

dramatically decreased to 0.5% of that of the wild type (see Supplemental Figure 5I online); this knockdown approached that of a *PFINV4* null-expression mutant, reflecting the existence of genetic interactions among MPF3 and *MPF2/PFINV4*. Concomitantly, we downregulated the *Physalis* phytoene desaturase gene (*PFPDS*) in an independent VIGS experiment as a control. We observed specific organ bleaching effects as observed in tomato when a phytoene desaturase gene was silenced (Liu et al., 2002), but we did not observe pollen defects and alterations in *PFINV4* expression (see Supplemental Figure 6 online), indicating the specificity of pollen defects in the manipulated genes. We therefore used a VIGS approach to confirm the genetic interactions between MPF3 and *MPF2*.

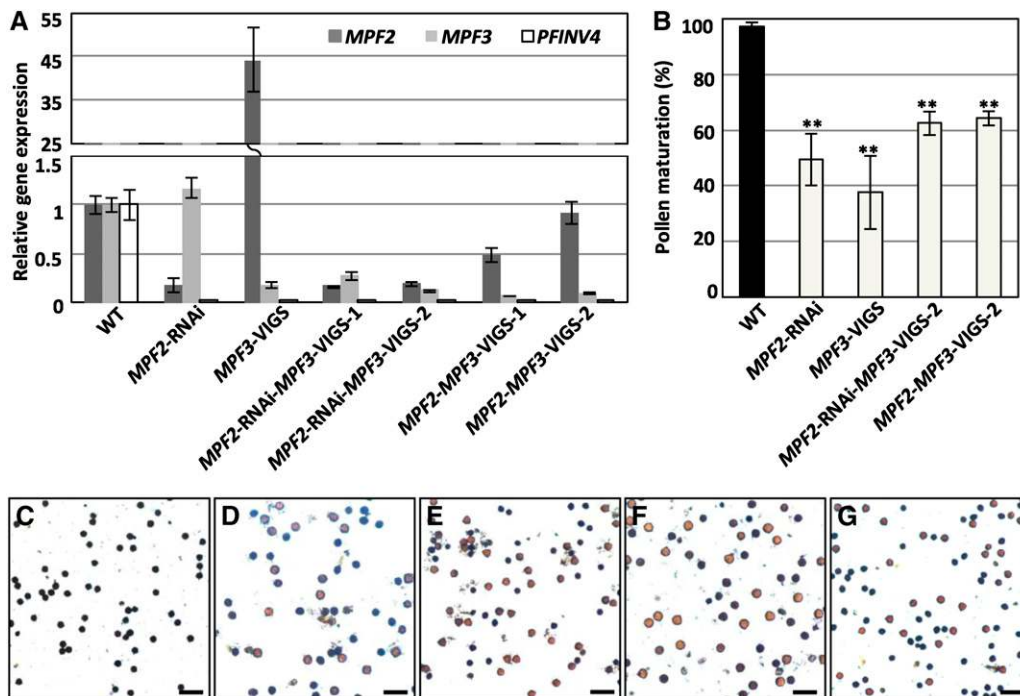### Genetic Interactions of *MPF3* and *MPF2* in Flower Development

To elucidate the genetic interactions between MPF3 and *MPF2*, double gene-silencing mutants of the two genes were created. We took advantage of the TRV-VIGS approach to silence *MPF3* in the KO38 line of *MPF2*-RNAi (He and Saedler, 2005) to generate *MPF2*-RNAi-*MPF3*-VIGS flowers. Concomitantly, we silenced both *MPF2* and *MPF3* in the wild type through VIGS to produce *MPF2*-*MPF3*-VIGS flowers. We genotyped the mutated

flowers using real-time RT-PCR (Figure 5A). In *MPF3* single downregulated mutants, the *MPF2* levels were dramatically elevated, while the expression of *MPF3* was not affected in flowers carrying a single *MPF2* mutation, indicating that *MPF2* is a downstream target of MPF3. Unlike their single silencing mutants, *MPF3* and *MPF2* expression levels were dramatically downregulated in the double mutants (Figure 5A). We then thoroughly characterized the silencing effects of the two genes on floral phenotypic variations.

Genetic Interaction between MPF3 and MPF2 Is Essential to Male Fertility

Male fertility is a primary role of a flower. A dramatic downregulation of *MPF2* blocks pollen production (He and Saedler, 2005). In the progeny of the KO38 line, some pollen grains were produced due to transgene silencing. However, in comparison with pollen maturation in the wild type (97.3% ± 2.8%; Figures 5B and 5C), only 49.4% ± 9.3% of pollen grains were found to be mature as revealed by I_2-KI staining (Figures 5B and 5D), suggesting that pollen maturation was significantly inhibited (P = 6.65×10^{-12}) by *MPF2* downregulation.

Once *MPF3* was silenced via the VIGS approach, 37.5% ± 13.2% of pollen reached maturity (Figures 5B and 5E), which is

Figure 5. The Role of Genetic Interactions between MPF3 and *MPF2* in Determining Male Fertility.

(A) Genotyping analysis. Expression of *MPF3* and *MPF2* in calyces and *PFINV4* in the androecium was revealed via real-time RT-PCR. The experiments were performed in biological triplicate. *Actin* was used as an internal control. Mean expression and SD are presented. WT, the wild type.

(B) Pollen maturation rate. For each genotype, 10 flowers were evaluated. The mean and SD are presented. Double asterisks indicate P < 0.01 in two-tailed Student's *t* test.

(C) to **(G)** I_2-KI–stained pollen from the wild type **(C)** and *MPF2* and/or *MPF3* downregulated flowers, as indicated (**[D]** to **[G]**). Active pollen is blue, and sterile pollen is yellowish-brown. Bars = 100 μm.

similar to the effect observed in *35S:MPF3*-RNAi lines (Figure 4O), indicating that pollen maturation processes were also significantly blocked (P = 4.04 × 10^{-11}) by the downregulation of *MPF3*. Nonetheless, in *MPF3* single downregulated mutants, *MPF2* was upregulated, hinting that poor male fertility might also result from a higher dosage of *MPF2* in the androecium. To verify the cause of immature pollen in *MPF3* single downregulated mutants, we assessed pollen maturation in *MPF2* and *MPF3* double downregulated flowers. We found that although the abnormality was alleviated (with ~65% of pollen reaching maturity; Figures 5B, 5F, and 5G), it was still significantly lower than in the wild type (P<2.57 × 10^{-14}). These findings suggest that both *MPF3* and *MPF2* directly regulate male fertility.

In all of these cases, stamen development was normal (see Supplemental Figure 3 online). However, *PFINV4* was markedly downregulated when either *MPF2* or *MPF3* was silenced (Figure 5A; see Supplemental Figure 4 online). Thus, abnormalities in male fertility in these mutant flowers may have resulted from

a dramatic suppression of *PFINV4*. These findings suggest that activation of *PFINV4* by interactions between MPF3 and *MPF2/MPF2* are essential for pollen maturation.

MPF3 Interacts Genetically with MPF2 to Specify the Identity of the Floral Calyx

Compared with the wild-type floral calyx (Figure 6A), knocking down of *MPF2* did not alter calyx identity (Figure 6B; He and Saedler, 2005). A dramatic downregulation of *MPF3* significantly altered the morphology of the calyx, which became more leaf-like (Figures 4 and 6C; see Supplemental Figure 5 online). In these cases, *MPF2* was upregulated in the floral calyx (Figures 4R and 5A; see Supplemental Figure 5H online). In our previous work, we discovered that overexpression of *MPF2* led to leaf-like calyces in *Solanum* (He and Saedler, 2005); therefore, we assumed that MPF2 was a key regulator of calyx organ identity. This assumption was validated in our double gene silencing analysis.
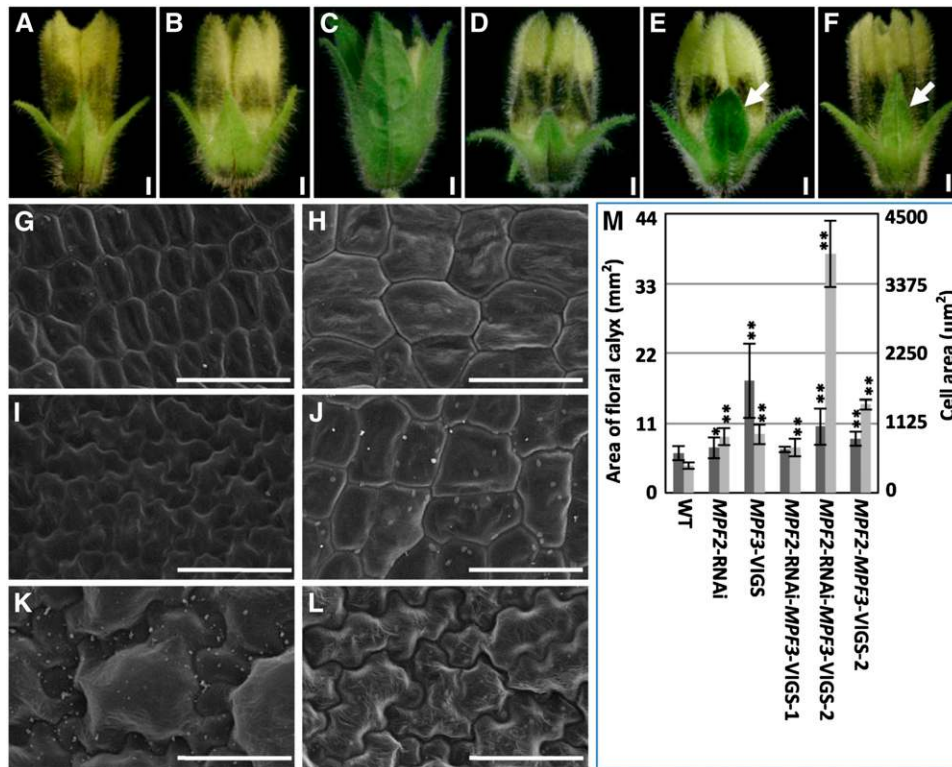
Figure 6. Both *MPF3* and *MPF2* Regulate Floral Calyx Identity.

(A) to **(F)** Phenotypic variation of the floral calyx. The white arrows indicate the leaf-like tip of calyces. Bars = 1 mm.
(A) The wild type.
(B) *MPF2*-RNAi.
(C) *MPF3*-VIGS.
(D) *MPF2*-RNAi-*MPF3*-VIGS-1.
(E) *MPF2*-RNAi-*MPF3*-VIGS-2.
(F) *MPF2*-*MPF3*-VIGS-2.
(G) to **(L)** Cell morphology of the floral calyx of the aforementioned phenotypes in **(A)** to **(F)**, respectively. Bars = 50 µm.
(M) Quantification of calyx size and the size of its respective cells (for details, see Supplemental Table 2 online). The genotype of each sample is referred to in Figure 5A.

Unlike the mutated flowers seen upon silencing of just *MPF3* (Figures 4 and 6C; see Supplemental Figure 5 online), we observed either no obvious alterations in calyx organ identity in the double gene downregulated flowers (i.e., *MPF2*-RNAi-*MPF3*-VIGS-1 flowers; Figure 6D) or only slight leaf-like structures in the tips of the floral calyces (as seen in *MPF2*-RNAi-*MPF3*-VIGS-2 and *MPF2*-*MPF3*-VIGS flowers; indicated by arrows, Figures 6E and 6F). In these cases, both *MPF3* and *MPF2* were knocked down (Figure 5A), implying genetic interactions between MPF3 and *MPF2* in the determination of calyx organ identity.

This observation was also supported by variations in epidermal cell morphology in the floral calyx (Figures 6G to 6L). Prior to anthesis, cells of the wild-type floral calyx were small and undifferentiated, with regular shapes (Figure 6G), while cells in the *MPF2*-RNAi floral calyx were significantly larger (P = 8.53×10^{-17}; Figure 6H). Cells also became significantly larger (P = 2.77×10^{-16}), irregular in shape typical of leaf cells on the floral calyx once *MPF3* was strongly downregulated (Figure 6I). This was accompanied by a dramatic elevation of *MPF2* transcript (Figures 4R and 5A; see Supplemental Figure 5H online). In *MPF2* and *MPF3* double knockdowns, consistent with variations in the morphology of the floral calyx (Figures 6D to 6F), two types of cell morphologies were observed. Cells on the *MPF2*-RNAi-*MPF3*-VIGS-1 flowers (Figure 6D) were even larger than those on the wild type, with a regular shape (Figure 6J), while cells of *MPF2*-RNAi-*MPF3*-VIGS-2 and *MPF2*-*MPF3*-VIGS flowers (Figures 6E and 6F) became larger than these of the wild type and irregular before anthesis (Figures 6K and 6L). These findings coupled cell identity with floral calyx identity, which are both governed by the repression of *MPF2* by MPF3. Interestingly, we discovered that the *MPF2*/*MPF3* transcript ratio in the floral calyx was important for cell identity (shape). When the ratio of *MPF2*/*MPF3* was greater than 1, cells were the shape typical of leaf cells, in comparison to the wild type.

The cell size within the floral calyx increased in all cases; however, the increase in cell size did not fully explain the variation in organ size (Figure 6M; see Supplemental Table 2 online). *MPF2* promotes cell division but inhibits cell expansion in the floral calyx (He and Saedler, 2005), but MPF3 negatively regulates the two processes. However, once both genes were downregulated, cells in the floral calyx became significantly larger (P<1.29×10^{-10}), while organ size was not altered (Figure 6M; see Supplemental Table 2 online); this suggested that cell division was basically inhibited. Therefore, genetic and physical interactions between MPF3 and MPF2 may promote cell division and inhibit cell expansion in the floral calyx.

These findings suggest that the repression of *MPF2* by MPF3 is a crucial step in specifying calyx identity and that their interactions also regulate cell division and expansion during the development of the floral calyx.

Both MPF3 and MPF2 Regulate Cell Division and Cell Expansion and, Thus, PostFloral ICS Size

Once cell identity is determined at the preanthesis stage, the ICS results from cell division and cell expansion. Cells in the mature ICS become irregular and dramatically expand. In the wild type, the ICS area increased ~46.1 ± 16.9 times, while cells in the ICS increased 10.9- ± 1.8-fold with respect to cells of the floral calyx. In contrast with the wild type (Figures 7A and 7G), with either *MPF2* or/and *MPF3* downregulated mutants, a smaller ICS was created after fertilization (Figures 7B to 7G); however, variation in cell size was quite complicated (Figure 7G; see Supplemental Figure 7 online). The variation in cell size did not completely explain the variation in organ size (see Supplemental Table 2 online). When the *MPF2*/*MPF3* ratio was smaller than one in comparison with the wild type (see Supplemental Figure 7A and Supplemental Table 2 online), significantly larger cells were found in the ICS, as in *MPF2*-RNAi (P = 3.81×10^{-7}; see Supplemental Figure 7B online) and *MPF2*-RNAi-*MPF3*-VIGS-1 (P = 3.29×10^{-14}; see Supplemental Figure 7D online), and cell division was thus suppressed. However, when the ratio was greater than 1, the cells of the ICS became significantly smaller (in the *MPF3*-VIGS and the *MPF2*-*MPF3*-VIGS-2; P = 0.00; Figure 7G; see Supplemental Figures 7C and 7F online) or were unaffected (in the *MPF2*-RNAi-*MPF3*-VIGS-2; P = 0.44; see Supplemental Figure 7E online); cell division was therefore enhanced. Hence, interactions between MPF3 and MPF2 may elegantly regulate cell division and cell expansion and regulate postfloral calyx growth, modulating the ultimate size of the ICS.

These results confirm that genetic interaction between MPF3 and *MPF2* is essential for male fertility, calyx identity,
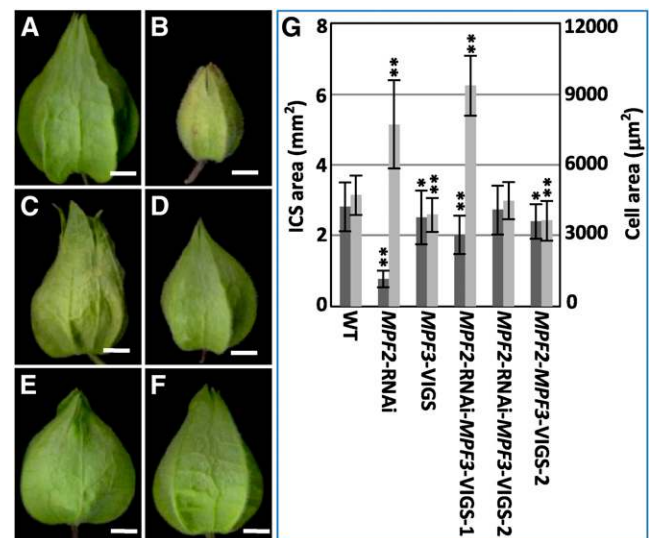
Figure 7. *MPF3* and *MPF2* Regulate Postfloral Calyx Size.

(A) to **(F)** Phenotypic variation of various ICSs. Bars = 5 mm.
(A) The wild type.
(B) *MPF2*-RNAi.
(C) *MPF3*-VIGS.
(D) *MPF2*-RNAi-*MPF3*-VIGS-1.
(E) *MPF2*-RNAi-*MPF3*-VIGS-2.
(F) *MPF2*-*MPF3*-VIGS-2.
(G) Quantification of ICS size and of its respective cells. Error bars are SD. Single and double asterisks stands for P < 0.05 and P < 0.01 in two-tailed Student's *t* test, respectively. (For details, such as sample sizes, see Supplemental Table 2 and Supplemental Figure 7 online.) The genotype of each sample is referred to in Figure 5A.

and ICS size in *Physalis* and suggest that protein–protein interactions between these two proteins affect these developmental processes.

Binding Capacity of MPF3-Associated Heterodimers to the CArG-Boxes in the *MPF2* Promoter

The CArG-box constitutes major binding sites for the MADS-domain transcription factors (West et al., 1997). However, no classical CArG motif, such as $CC(A/T)_6GG$ and $C(A/T)_8G$, is present in the 1.4-kb *MPF2* promoter region (He and Saedler, 2005). The promoter was then extended to 2.5 kb upstream of the translation initiation site (Riß, 2009; Khan et al., 2012), and sequence analysis revealed different types of CArG-boxes, including two $CC(A/T)_6GG$, one $C(A/T)_8G$, and one $CC(A/T)_7G$ (Figure 8A; see Supplemental Table 3 online). In addition, two variants $C(A/T)_7GG$ were found in the 5′-untranslated region. Altogether six motifs were designated as M1 to M6 in ordered sequence (Figure 8A; see Supplemental Table 3 online). Therefore, we assumed that MPF3 and its associated heterodimers fulfilled their biological functions by selectively binding to some of these motifs. To test this hypothesis, we conducted electrophoretic mobility shift assays (EMSAs).

Dimerization of MADS-domain proteins is required for DNA binding (Immink et al., 2010). Since these proteins can homodimerize, we first evaluated the binding ability of the homodimers to these CArG-boxes and found that MPF2 homodimers bound to the first three CArG-boxes (i.e., M1, M2, and M4) in the *MPF2* promoter (Figure 8C) and that PFAG homodimers could bind to M1 and M4 (Figure 8G). By contrast, homodimers of MPF3, PFGLO1, and PFGLO2 were not able to bind to any of the CArG-boxes (Figures 8B, 8E, and 8F). Next, we monitored ability of MPF3-associated heterodimers to bind to these CArG-boxes. We demonstrated that MPF3-MPF2 heterodimers selectively bound to M1 and M4 (Figure 8D); MPF3-PFAG bound to M4, M5, and M6 (Figure 8J); and MPF3 and PFGLO1/PFGLO2 heterodimers did not bind with any of these motifs (Figures 8H and 8I). Thus, these DNA binding activities provide a basis for the regulation of *MPF2* by the related protein dimers and specifically for the genetic interaction between MPF3 and *MPF2* in floral organs.

MPF3 appears to have secured novel floral roles through the evolution of novel physical and genetic interactions, which largely result from alterations in its coding regions, as it features an expression pattern similar to that of the other *euAP1* genes. This was further supported by selection analysis and a functional proof using a transgenic heterologous host.

Positive Selection of MPF3 Supports Its Functional Diversification

The sequence diversification of euAP1 was evaluated via selection analysis. The sequences with known functions from Brassicaceae, Fabaceae, Plantaginaceae, and Solanaceae were included for selection tests using two types of models (branch and branch-site models). In the free ratios branch model test (model = 1, giving separate ω values for each branch), the MPF3 branch was detected as having significant positive selection
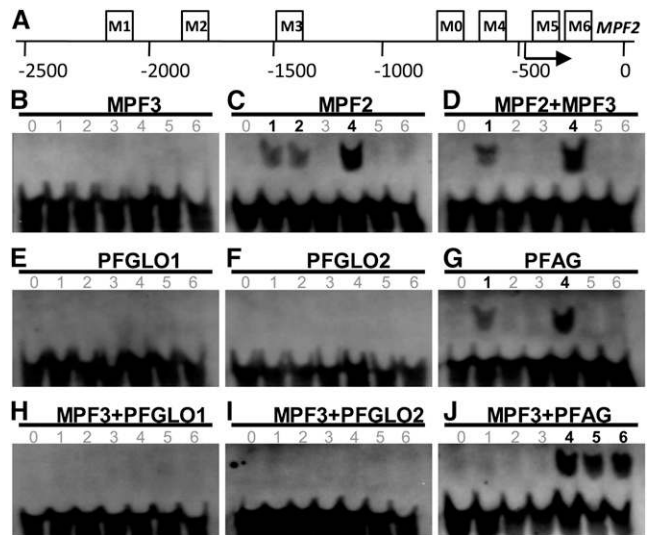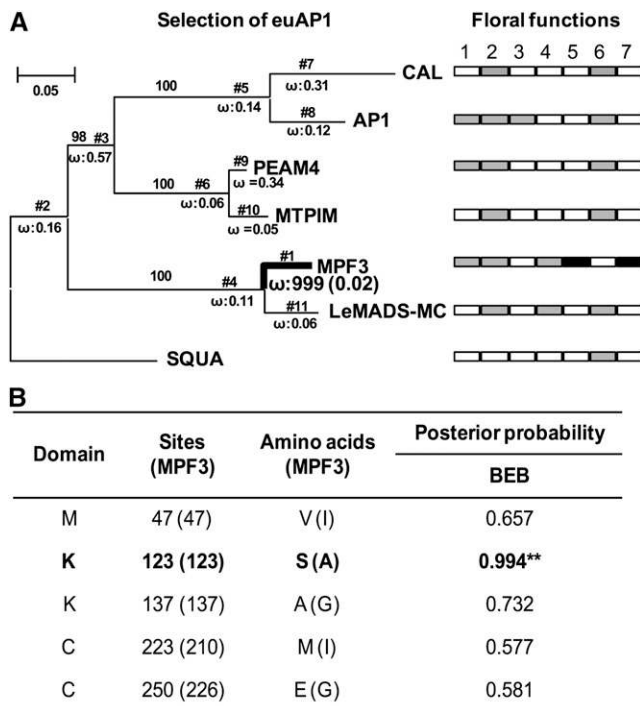

Figure 8. Ability of the MPF3 Interacting Partners and the Associated Heterodimers to Bind to a CArG-Box in the *MPF2* Promoter.

(A) Distribution of CArG-box variants in the *MPF2* promoter. M1 to M6 designate the CArG-boxes and M0 the random non-CArG-box as a negative control in the EMSA. The arrow indicates the putative transcriptional initiation site (He and Saedler, 2005). Position 0 indicates the translational start site. The boxes stand for M0 to M6 motifs and their relative positions on *MPF2*. For sequence details, see Supplemental Table 3 online.

(B) to **(J)** EMSA results of the MADS-domain protein binding to the CArG-boxes in the *MPF2* promoter. The numbers from 0 to 6 indicate M0 to M6, respectively. Numbers in black and bold stand for the CArG-box bound by the indicated MADS-dimers, and the numbers in gray represent the motif that cannot be bound by the indicated MADS-dimers.

(B) MPF3.
(C) MPF2.
(D) MPF3 and MPF2.
(E) PFGLO1.
(F) PFGLO2.
(G) PFAG.
(H) MPF3 and PFGLO1.
(I) MPF3 and PFGLO2.
(J) MPF3 and PFAG.

(ω = 999; highlighted with bold lines, Figure 9A). When all branches were set as foreground branches, the branch model test (model = 2, giving different ω values between foreground and background branches) further confirmed this (see Supplemental Table 4 online). Furthermore, to uncover the positive sites in MPF3, the branch-site model test was executed; this allows positive selection at a small number of sites along a specific lineage and is the most powerful model to detect positive selection. In this test, the MPF3 branch in euAP1 was set as the foreground branch, and five potential sites were found to be under positive selection. Notably, these sites were all distributed in the M, K, and C domains; in particular, Ala-123 in the K domain had a high posterior probability (Figure 9B). This evidence suggests that functional differentiation in these sites may be associated with alterations of MPF3 in DNA binding ability and protein–protein interactions during evolution.

A

B

Domain	Sites (MPF3)	Amino acids (MPF3)	Posterior probability BEB
M	47 (47)	V (I)	0.657
K	**123 (123)**	**S (A)**	**0.994****
K	137 (137)	A (G)	0.732
C	223 (210)	M (I)	0.577
C	250 (226)	E (G)	0.581

Figure 9. Positive selection of MPF3 supports diversification of its floral functions.

(A) The bold line indicates that positive selection was detected in the branches or the proteins. The proportion of sites with ω > 1 for the foreground branches is indicated under the branches in the bracket. SQUA was used as outgroup. Floral functions include (1) flowering time, (2) sepal identity, (3) petal identity, (4) calyx size, (5) ICS formation, (6) inflorescence or floral meristem, and (7) male fertility. As indicated, the gray box designates the genes that possess the role, while the empty box depicts the absence of such a role. The novel role for MPF3 is highlighted by the black box.
(B) Selectively relaxed constrained sites in MPF3. The sites and amino acids in parentheses are relative to those in MPF3. Bold font and asterisks indicate a positively selected codon site having P > 95% in Bayes Empirical Bayes (BEB) analysis.
[See online article for color version of this figure.]

Our selection results support functional differentiation of MPF3 in comparison with other euAP1 members, and we show that *euAP1* genes from various genera encode MADS-box proteins with multiple functions. The floral roles for each gene in its own native host vary and include flowering time, sepal identity, petal identity, calyx size, ICS formation, floral/inflorescence meristem, and male fertility (Figure 9A). MPF3 appears to have secured a novel role in male fertility and ICS formation in *Physalis*.

Functional Divergence Is More Pronounced in a Transgenic Heterologous Host

We pose the following questions. How does sequence divergence under positive selection affect the functional divergence of euAP1 between Solanaceae and Brassicaceae? As orthologs of AP1, do MPF3 from *P. floridana* and its ortholog St-*MC* from *Solanum*

tuberosum really function as AP1 does in *Arabidopsis*? To answer these questions, we overexpressed the two genes in *Arabidopsis* and its *ap1* mutants, respectively. At least 15 independent transgenic lines were obtained for each construct and showed similar phenotypic variations. Single transgenic lines for St-*MC* and for *MPF3* were characterized in a wild-type *Arabidopsis* background via DNA gel blot analysis. The bolting time and rosette leaf number at the time of bolting under either long-day or short-day conditions were recorded as the flowering time. In both conditions, the plants harboring St-*MC* or *MPF3* had a flowering time comparable to that of wild-type *Arabidopsis*, while *35S:AP1* transgenic plants apparently flowered earlier (see Supplemental Figure 8 online), indicating that *MPF3* and St-*MC* did not promote earlier flowering in *Arabidopsis*. In an *ap1* background (three different alleles *ap1-1*, *ap1-10*, and *ap1-12* were used), neither protein complemented the floral phenotype of these *ap1* mutants. These results suggest that orthologs of euAP1 from Solanaceae and Brassicaceae, which are separated by a great evolutionary distance, underwent functional divergence. We therefore reiterate that using a heterologous system, such as *Arabidopsis*, is not the best method to evaluate gene function and the evolution of gene function.

DISCUSSION

Gene duplication events have occurred at least twice during the evolution of the *AP1/SQUA*-like genes, resulting in the *euFUL*, *FL*, and *euAP1* subclades in eudicots (Becker and Theissen, 2003; Litt and Irish, 2003; Shan et al., 2007). Within Solanaceae, an additional duplication event resulted in two copies (*PFFUL1/2*) of *euFUL*. Although these paralogs became diversified in sequence and expression, they are expressed in floral organs and possess diverse functions (Litt, 2007). The euAP1 have drawn more attention because of their role in the specification of sepal organ identity in flower development (i.e. AP1 in *Arabidopsis* [Mandel et al., 1992] and Le-MADS-MC in *Solanum* [Vrebalov et al., 2002]); therefore, their orthologs might have played a role in the evolution of the Chinese lantern or ICS. Four *AP1/SQUA*-like homologs were isolated in *Physalis*, and we demonstrated an essential role for MPF3 in flower development. As a *euAP1* member, the prevalent expression of *MPF3* in the floral meristem appears to support the hypothesis that MPF3 specifies floral meristem identity and regulates flowering time. Constitutive expression of *MPF3* indeed promoted flowering in transgenic *Physalis*, while specific silencing analyses revealed that these roles were likely redundant or insignificant. MPF3 regulates floral calyx identity and growth and has novel functions in flower development through genetic and physical interactions with the key components of both postfloral ICS and male fertility (Figure 10A). This protein thus couples the two developmental processes of both ICS and male fertility during the evolution of *Physalis*.

Genetic Regulation of MPF3 and *MPF2* Primarily Specifies Floral Calyx Identity

MPF3 primarily determines calyx organ identity, since its knockdown leads to a leaf-like calyx and its orthologs from various

plant species regulate sepal organ identity (Mandel et al., 1992; Gustafson-Brown et al., 1994; Berbel et al., 2001; Taylor et al., 2002; Vrebalov et al., 2002; Benlloch et al., 2006). MPF3 is distinct from AP1 in *Arabidopsis*, but similar to other euAP1 genes, and does not control petal organ identity; however, it is expressed in corolla and corolla primordia during floral development. The role of *MPF3* in corolla development might be redundant or partitioned by its paralogs, as was recently observed in poppy (*Papaver somniferum*, Pabón-Mora et al., 2012). In addition, MPF3 may not repress the expression of a C-function gene (*PFAG*) since *PFAG* is expressed in the gynoecium and its primordia, where the C-function gene exerts its role. Thus, MPF3 partially serves as an A-function gene to regulate calyx organ identity. The concept of the floral A-function has been problematic since its inception (Schwarz-Sommer et al., 1990; Litt and Irish, 2003; Litt, 2007). Our findings provide additional evidence to challenge an evolutionary conservation of the A-function gene as defined in *Arabidopsis* (Coen and Meyerowitz, 1991; Weigel and Meyerowitz, 1994). The controversy regarding the A-function appears to resolve when subfunctionalization after gene duplications is considered (Litt and Kramer, 2010; Pabón-Mora et al., 2012). Regardless, the core role of the A-function is to specify sepal identity.

Alteration of sepal identity often accompanies alteration of cell morphology or identity; for example, trichome type is a typical morphological marker used to distinguish the sepal and leaf in *Arabidopsis* (Mandel et al., 1992; Gustafson-Brown et al., 1994). However, cell morphology is not necessarily considered to be a marker that distinguishes the calyx and leaf in Solanaceae (Hu and Saedler, 2007). The epidermal cells on the floral calyx stay undifferentiated and are smaller prior to anthesis in *Physalis* and then differentiate to be lobate in the postfloral calyx. However, in the *MPF3*-silenced mutants, the cell morphology of the transformed calyx before anthesis was already strongly lobate (as with cells making leaves), indicating that MPF3 specifies calyx identity by regulating cell identity. According to the floral quartet model (Theissen and Saedler, 2001), interaction with SEPALLATA-like proteins in *Physalis* (PFSEPs) (e.g., PFSEP1, PFSEP2, and PFSEP3; He et al., 2007) appears to be sufficient for MPF3 to specify calyx identity (Figure 10A).
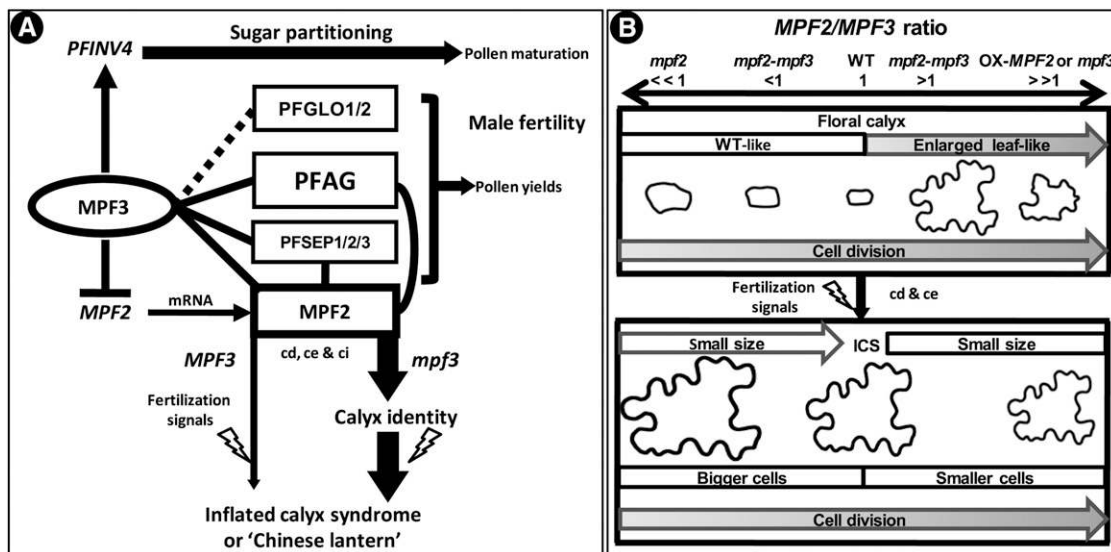
Figure 10. Summary of Floral Calyx and Postfloral ICS Development in *Physalis*.

(A) Current integrated MPF3-associated regulatory and interacting networks for ICS development in *Physalis*. The networks summarize knowledge gained from previous studies (He and Saedler, 2005; He and Saedler, 2007; He et al., 2007; Zhang et al., 2012) and this article. Proteins are presented in vertical circles or boxes, and genes or mRNAs are in italics. The solid lines indicate protein–protein interactions, while the dashed line indicates that the interactions need to be verified. Arrows stand for activation or promotion, and blocked lines for repression. cd, cell division; ce, cell expansion; ci, cell identity. The lightning symbol represents fertilization signals. For details, see text.

(B) The *MPF2/MPF3* ratio model in the development and growth of the floral calyx and ICS in *Physalis*. Calyx development after primordia initiation consists of (top portion) the stage that organ identity is determined, organ growth before flowering, and (bottom portion) postfloral calyx outgrowth, which is triggered by fertilization signals (lightning symbol). The *MPF2/MPF3* ratio is proposed to play an important role in these processes, particularly in establishing the identity of the floral calyx. MPF2 and MPF3 also regulate cell division and cell expansion in floral and postfloral calyx growth. Cell size and cell morphology are given proportionally for each context. Cell size for the fruiting calyx is ~11 times that in the floral calyx, while the ICS area is ~46 times that of the floral calyx area, indicating that ICS is a result of cell division (cd) and cell expansion (ce). WT, the wild type; *OX-MPF2*, *MPF2* overexpression line; *mpf2*, *mpf3*, and *mpf2-mpf3*, downregulation mutants. The *MPF2/MPF3* ratio in the wild type is set to 1; in the mutants, the ratio is then either >1 (>>1) or <1 (<<1). Shaded arrows in the floral calyx context represent a gradual promotion of the corresponding trait. Empty arrows in the ICS context depict a severe downregulation of either *MPF2* or *MPF3*, which results in flowers with a smaller ICS than in those of the wild type. When the ratio is <1, larger cells are produced, whereas a ratio >1 results in smaller cells. This model is based on the quantification of cell and organ size of the transgenic mutants in comparison with the wild type (summarized in Supplemental Table 2 online).

However, the precise specification of floral calyx identity might also require the activity of MPF2, which has a dose-dependent effect (Figure 10B). Overexpression of *MPF2* in *Solanum* (He and Saedler, 2007), similar to the overexpression of its ortholog, *AGL24*, in *Arabidopsis* (Yu et al., 2004), superimposed a vegetative developmental program in flower development and generated leaf-like sepals, phenocopying *ap1* mutants and indicating that the repression of *AGL24* is a crucial step in promoting flower development (He et al., 2004; Yu et al., 2004). By analogy, MPF3 (the ortholog of AP1) was thought to repress *MPF2*, while variation in the promoter of *MPF2* led to heterotopic expression of the gene itself in floral organs (He and Saedler, 2005); however, the native expression of *MPF2* in the calyx may be too low to alter the identity of the floral calyx in *Physalis*. In *MPF3*-silenced flowers, however, *MPF2* expression was more than 10 times greater than in the wild-type calyx, as in lines that overexpress *MPF2*, which led to a change in the identity of the calyx and its cells (Figure 10). When both *MPF3* and *MPF2* were silenced, no obvious leaf-like calyx was seen or only a weak homeotic transformation in the calyx tips was observed. Thus, the *MPF2/MPF3* ratio was critical for specifying the floral calyx identity (Figure 10B). Once the ratio was greater than 1, the vegetative growth in calyx development was superimposed and a leaf-like floral calyx was created; otherwise, the calyx was determined. These findings confirm the role of genetic control of *MPF2* by MPF3 during floral development.

There is no classical CArG-box present in the 1.4-kb *MPF2* promoter (He and Saedler, 2005), but some variants exist near the transcriptional initiation site, and three classical CArG-boxes occur in a remote region (Riß, 2009; Khan et al., 2012), providing the structural basis for a direct genetic interaction between MPF3 and *MPF2*. Our EMSA revealed that MPF2 bound to M1, M2, and M4 and that MPF3 itself cannot bind to any CArG-box of the *MPF2* promoter. However, MPF3-MPF2 selectively bound to M1 and M4, indicating that expression of *MPF2* was at least self-regulated and that the floral organs were more tightly regulated by MPF3-MPF2 together than by MPF3 alone. M1 bound by MPF3 seems to repress *MPF2*, since the CC(A/T)$_7$G CArG-box (designated as M4) in the vicinity of the transcriptional initiation site might contribute to the heterotopic expression of *MPF2* in floral organs, which was also proposed for *MPF2-like* expression in sepals (Khan et al., 2012). The M4 site may result from a point mutation in the classical CArG boxes [either CC(A/T)$_6$GG or C(A/T)$_8$G] or from a unique origin in *Physalis*. *In Solanum*, the M4 motif is missing and the activation of *STMADS16* by St-MC is abolished in the floral organs (He and Saedler, 2005; Riß, 2009; Khan et al., 2012). By contrast, in *Physalis* (very likely due to presence of the M4 motif), *MPF2* is activated by MPF3; hence, *MPF2* is heterotopically expressed in floral organs.

Thus, the complex of MPF3 and PFSEPs regulates calyx identity by interacting directly with *MPF2*/MPF2 either genetically or physically in *Physalis* (Figure 10A), similar to the situation suggested for the orthologous pair AP1-*AGL24* in *Arabidopsis* (Yu et al., 2004; de Folter et al., 2005). Our results indicate that the key regulatory networks involved in sepal organ identity are evolutionarily conserved across plant families and further suggest that a mutation or evolution of a key regulatory element in a key gene alters gene expression to dramatically shape the morphology in Solanaceae.

MPF3 and MPF2 Regulate Cell Cycle Processes in Calyx Growth, Thus Determining ICS Size

Organ growth is the result of cell division and cell expansion. In *Physalis*, calyx growth can be divided into floral and postfloral processes. In both cases, the *MPF2/MPF3* ratio is associated with cell cycle processes (Figure 10B). In our study, cell division was promoted as the ratio increased; thus, MPF2 is the major determinant promoting cell division, while MPF3 inhibits cell division during both developmental processes in the calyx of *Physalis*. However, the cell size changes in the downregulated mutants proved to be quite interesting.

During floral development, cell size in the calyx increased if either *MPF3* or *MPF2* was downregulated (Figure 10). Thus, both MPF3 and MPF2 act as repressors of cell expansion in the growth of the floral calyx. Although downregulation of *MPF2* increased cell size, the unaffected *MPF3* inhibited cell division; thus, floral calyx size was largely unaffected. Once *MPF3* was knocked down, the concentration of *MPF2* mRNA was significantly elevated. Thus, the rate of cell division and cell size both increased, and the floral calyx was transformed into an enlarged leaf-like organ. In the double downregulated mutants, the ratio of *MPF2/MPF3* varied. Once again, when the ratio was under 1, the cells were enlarged, while when the ratio was greater than 1, the cell size fluctuated, but was still much larger than in the wild type. This implies a physical interaction between MPF2 and MPF3 (in addition to their genetic interaction) in the growth of the floral calyx.

In contrast with the floral calyx, once *MPF3* was downregulated, the size of the mature ICS and its cells was reduced, indicating that MPF3 promoted cell expansion in the fruiting calyx. Opposite effects on cells were observed once *MPF2* was knocked down (He and Saedler, 2005), but this also resulted in a smaller lantern. In the absence of *MPF3* and with a dramatic increase in *MPF2* mRNA, cell size was reduced and this resulted in a smaller ICS. Moreover, cell expansion in the fruiting calyx was also regulated by the *MPF2/MPF3* ratio in the double-silenced mutants (Figure 10B). Cells were larger than wild-type cells when the ratio was less than one and smaller when the ratio was greater than one. However, the ICS became smaller once either of the two genes was downregulated. Thus, both MPF3 and MPF2 and their interactions are essential to the final size of the Chinese lantern in *Physalis*.

The molecular details regarding how MPF3 and MPF2 regulate the cell cycle in the development and growth of both the floral calyx and postfloral calyx are not yet understood; however, floral transcriptomic comparisons between the wild type and various mutants could improve our understanding of these processes. However, abundance and dosage balance of MPF2 and MPF3, and their genetic and physical interactions, regulate cell division, cell expansion, and cell differentiation. Interactions with fertilization or hormonal signals ultimately trigger postfloral calyx outgrowth and the development of ICS (He and Saedler, 2005; He and Saedler, 2007) and might relate to male fertility.

Both MPF3 and MPF2 Are Integral to Male Fertility

Stamen identity is regulated by B-, C-, and E- function proteins (Theissen and Saedler, 2001). The euAP1 genes are not involved

in this developmental process, since mutations of these genes do not affect male fertility. Although silencing of *MPF3* did not affect anther development, pollen maturation was severely impaired, which affected male fertility. *MPF3* is expressed in androecium primordia during early floral development; however, its expression drops once the androecium is formed. One possibility is that the earlier expression might impact pollen development. Alternatively, the low level could still be enough to direct pollen maturation. Furthermore, a discrepancy between mRNA expression and protein expression might also play a role (Immink et al., 2010). Finally, as reported previously (Wu et al., 2003; Urbanus et al., 2009, 2010), the possibility of both intercellular transport of MPF3 and non-cell-autonomous function cannot be excluded. Nevertheless, all of the above could essentially alter the effect of MPF3 on pollen development.

MPF2 knockdown results in male infertility primarily due to a dramatic reduction in pollen yield (He and Saedler, 2005). The defects in pollen maturation in successive generations resemble those in *MPF3*-silenced lines. However, downregulation of *MPF3* resulted in increased expression of *MPF2* in the androecium, indicating that *MPF2* overexpression could also damage pollen maturation. A similar defect in pollen development was seen in *MPF2 MPF3* double knockdowns, although more pollen grains appeared to be normal. Therefore, the activity of both MPF3 and MPF2 is required for normal pollen development (Figure 10A).

MPF2 may affect male fertility by interacting with florally expressed MADS-domain proteins in *Physalis* (He et al., 2007). Thus, both interactions with other MADS-domain proteins and the regulation of their target genes are important but not essential for MPF3 to affect male fertility. GLO in *Antirrhinum* (a B-function protein; Tröbner et al., 1992), TM29 (a SEP-like protein, E-function) in *Solanum* (Ampomah-Dwamena et al., 2002), and FARINELLI (C-function) in *Antirrhinum* (Davies et al., 1999) are all involved in male fertility. Since MPF3 and MPF2 interact with their orthologs, including PFGLO1, PFGLO2, PFSEP2/3, and PFAG (this study; He et al., 2007), the roles of these orthologs in male fertility should also be considered. The interactions between MPF3 and PFAG and MPF2 seem to be weak but stable, since they were detected in vitro and in vivo. Direct interactions between euAP1 proteins and B-function proteins have not yet been reported in angiosperms. Even Le-MADS-MC from *Solanum*, a close relative of *Physalis*, does not show this capability (Leseberg et al., 2008). We demonstrated that MPF3 interacts weakly with PFGLO1 and PFGLO2 in vitro, but no YFP signal was detected in our BiFC analyses using plant leaf cells. Thus, such interactions might also be transient in *Physalis*. Coexpressing these proteins in a plant cellular environment allows for various putative partners with stronger attractions for these MADS-domain proteins to become available and compete with each other for dimerization and complex formation (Immink et al., 2010), thus abolishing any YFP signal. The molecular details regarding this hypothesis need to be extensively investigated. Nonetheless, the stable and transient protein–protein interactions of both MPF3 and MPF2 with these male fertility–associated MADS-domain proteins could together affect the dynamics of the quartet determining the stamen (Theissen and Saedler, 2001), and this might make it essential for MPF3 and MPF2 to influence pollen yields and maturation in *Physalis*

(Figure 10A), as observed in the previous work (He and Saedler, 2005) and in this work.

In a parallel fashion, Suc accumulation in pollen grains is essential for pollen maturity (Ranwala and Miller, 1998; Oliver et al., 2005; Zhang et al., 2010). In our study, insufficient sugar accumulated in the pollen grains once either *MPF3* or *MPF2* or both were knocked down. Expression of several related genes was monitored and *PFINV4* was concomitantly, specifically, and strongly repressed in the androecium. Its ortholog *INV4* in *Oryza* and *Lilium* was demonstrated to be a key component in sugar partitioning during anther development (Ranwala and Miller, 1998; Oliver et al., 2005). Thus, it is likely that the marked downregulation of *PFINV4* causes an abnormal photosynthetic carbon allocation, leading to immature pollen grains. Thus, MPF3, by interacting with MPF2, may activate the *PFINV4* gene to regulate male fertility by affecting sugar partitioning (Figure 10A). In particular, PFAG could bind to the CArG-boxes, M1 and M4, and MPF3-PFAG could bind to the CArG-boxes, M4, M5, and M6, in the upstream regions of *MPF2*. It is interesting that PFAG and MPF3-PFAG share a CArG-box M4 with MPF2-MPF3 and MPF2. Moreover, MPF3-PFAG could bind to variants of CArG-boxes in the 5′-untranslated region. Although the biological relevance of these interactions needs to be substantiated, these findings indicate that PFAG and MPF3-PFAG also fulfill a role in this pathway that may be mediated by *MPF2*. However, PFGLO1, PFGLO2, and their MPF3-associated heterodimers did not bind to any CArG-boxes of the *MPF2* promoter; thus, they might not affect male fertility via direct genetic interaction with *MPF2*. Whether they also regulate *PFINV4* in this novel pathway by MADS-domain transcription factors needs to be further investigated.

Therefore, MPF3 has an integral role in male fertility without affecting stamen organ identity and development. The MPF3-MPF2/*MPF2*–regulating and –interacting complex, as a primary regulator of cell division and cell expansion, is integrated into the male fertility–determining networks through novel genetic and physical interactions. This integration further corroborates the previous assumption of the role of male fertility in the evolution and development of the ICS (He and Saedler, 2005; He et al., 2007).

Therefore, MPF3 may orchestrate floral initiation and ICS formation by integrating identity, growth, patterning, and hormonal pathways in *Physalis*, as suggested for AP1 in *Arabidopsis* (Kaufmann et al., 2010), but it has acquired novel and essential functions in ICS formation and male fertility. The latter findings are different from data obtained for other euAP1 genes (Figure 9), and functional divergence within the euAP1s in floral development is also discussed below.

Positive Selections Underlie Functional Diversification of euAP1 Orthologs

Several *euAP1* family members from various genera have been functionally characterized thus far, such as *AP1* and *CAL* in *Arabidopsis* (Mandel et al., 1992; Bowman et al., 1993), *SQUA* in *Antirrhinum* (Huijser et al., 1992), Le-*MADS-MC* in *Solanum* (Vrebalov et al., 2002), *PEAM4* in *Pisum* (Berbel et al., 2001; Taylor et al., 2002), *MTPIM* in *Medicago* (Benlloch et al., 2006), and *MPF3* in *Physalis* (this study). In addition to *SQUA*, other

molecules play a role in sepal identity, and the divergences between *MPF3* and other *euAP1* genes are apparent due to the functional pleiotropic processes of the involved genes (Figure 9).

Particular functions have been ascribed to some orthologs; for example, the role in petal development seems to be unique for AP1 in *Arabidopsis* (Mandel et al., 1992; Bowman et al., 1993). The functional divergence is more pronounced when euAP1s from different plant families are heterologously tested in the same system (e.g., *Arabidopsis* from Brassicaceae). In addition to its role in floral organ identity, AP1 plays an important role in the fate of the floral meristem, as revealed by loss-of-function studies (Mandel et al., 1992; Bowman et al., 1993; Yu et al., 2004), and a gain-of-function mutation of *AP1* promotes flowering in *Arabidopsis* (Mandel and Yanofsky, 1995) and in a heterologous host (Peña et al., 2001). However, both *MPF3* and St-*MC* from Solanaceae failed to complement *ap1* mutants, and their overexpression in wild-type *Arabidopsis* did not lead to earlier flowering. Therefore, we emphasize that the function of a gene should be inferred in its native host.

Nearly all euAP1s reported affect floral or inflorescence meristem identity in their own hosts (Figure 9; Huijser et al., 1992; Mandel et al., 1992; Taylor et al., 2002; Vrebalov et al., 2002; Berbel et al., 2001; Benlloch et al., 2006). However, solitary flowers with a leaf-like calyx are seen in *35S:MPF3*-RNAi *Physalis*, indicating that floral meristem identity is not altered by knocking down *MPF3*. The low abundance of *MPF3* transcript in the *MPF3* knockdowns may be sufficient to promote flower development; conversely, the role of *MPF3* in floral meristem identity may be shared with its paralogs. Studies of *mpf3* null mutants and genetic analyses of *MPF3* and its paralogs in *Physalis* could resolve this.

Even within the family Solanaceae, euAP1 from different genera behave differently. *Solanum* is a close relative of *Physalis*, since the microsynteny is well maintained for the *MPF3* orthologs in *Physalis* and Le-*MADS-MC* orthologs in *Solanum*. Loss of Le-*MADS-MC* in tomato led to a leaf-like macrocalyx and altered the determinacy of the inflorescence (Vrebalov et al., 2002); however, this gene is not involved in male fertility as *MPF3* is in *Physalis*.

MPF3 shares a similar expression domain with other *euAP1s* (Huijser et al., 1992; Mandel et al., 1992; Carr and Irish, 1997; Vrebalov et al., 2002) that are exclusively expressed in floral development. Thus, their functional divergence mainly results from variations in their coding regions. MPF3 underwent strong Darwinian selection, and the five selected sites located in the M, K, and C domains (Figure 9) might alter the spectrum and strength of the target genes and protein–protein interactions, thus resulting in functional divergence. In particular, site 123 (with Bayes Empirical Bayes > 0.95) in the K domain, which is known to regulate protein–protein interactions (reviewed in Immink et al., 2010), seems to be critical for the divergence of protein–protein interactions. The lower probability of the other sites undergoing selections indicates that they might play a lesser role in affecting the protein–protein interactions. In accordance with this, we observed that the interacting protein spectrum differed in different species. The euAP1 orthologs, as observed for both AP1 in *Arabidopsis* (de Folter et al., 2005) and Le-MADS-MC in *Solanum* (Leseberg et al., 2008), did not interact with any B- and C-function proteins, while SQUA in

Antirrhinum (Davies et al., 1996) and MPF3 in *Physalis* interacted with C-function proteins. MPF3 interacted with B-function proteins only in *Physalis*. Positive selection in protein sequences might also have led to the evolution of novel regulatory pathways. As we have demonstrated, MPF3 evolved its regulatory role in sugar partitioning pathways most likely by activating *PFINV4*, and MPF3 was involved in the origin of the ICS by interacting with *MPF2*/MPF2 (Figure 10A). Such a specific interaction and its effects on pollen maturation have not been observed in other euAP1 mutants.

Thus, changes in the molecular interaction networks of MPF3 in comparison to the molecular interaction networks of its orthologs may form the basis for the diverse phenotypic variations observed in the *MPF3*-silenced mutants. The roles of euAP1 proteins have diversified, and this diversification is undoubtedly driven by the action of different selective pressures during evolution.

Conclusions

Although the expression domains of euAP1 proteins are basically identical, these proteins, under positive selection, underwent functional diversification during the course of evolution. Nonetheless, most of the euAP1s are determinants of sepal identity. The formation of the novel trait, the Chinese lantern, in *Physalis* is not a result of a change in organ identity. The MPF3-*MPF2* regulatory circuit is associated with cell division, cell expansion, and cell identity, and this circuit thus regulates floral calyx development and postfloral outgrowth to an ICS (Figure 10B); however, the evolution of the circuit's interactions with PFAG, PFGLO1/2, and PFSEP1/2/3 implicates it in male fertility (Figure 10A). The evolution of a role in regulating the sugar partitioning pathway through the activation of *PFINV4*, which encodes an invertase, suggests that *MPF3*, a *euAP1* MADS box gene, is associated with stamen functionality. The involvement of MPF3 and MPF2, as key regulators in calyx development, in male fertility seems to be integral to the origin of the Chinese lantern, since a fertilization signal is required for the development of this novel trait (He and Saedler, 2005; He and Saedler, 2007). Thus, the regulation of these identified MADS box genes and interactions among their proteins as determined by this study and others (He and Saedler, 2005; He et al., 2007), are involved in the evolution and development of the postfloral novelty, the Chinese lantern or ICS, in *Physalis*.

METHODS

Plant Materials

Solanum macrocarpon, potato (*Solanum tuberosum*), and *Arabidopsis thaliana* were grown in greenhouses at the Max-Planck Institute for Plant Breeding Research (Cologne, Germany) under long-day or short-day conditions. *Physalis floridana* P106 (He and Saedler, 2005) was grown in a growth chamber at the State Key Laboratory of Systematic and Evolutionary Botany of the Chinese Academy of Sciences (Beijing, China) under long-day conditions. The lines of three different alleles of *ap1* mutants (*ap1-1*, *ap1-10*, and *ap1-12*) and a *35S:AP1* transgenic *Arabidopsis* were purchased from The Arabidopsis Information Resource (http://www.Arabidopsis.org/). Leaves and floral materials were harvested for genomic DNA and total RNA isolation.

Gel Blot Analyses

RNA and DNA gel blot analyses were performed as previously described (He et al., 2002). For RNA hybridization, the *Actin* gene was reprobed as a loading control after the filters were stripped. *MPF3* cDNA fragments encoding the C-domain and the 3′-untranslated region were used as probes for both RNA and DNA gel blot hybridizations in *Physalis*. A *MPF3* cDNA fragment or a corresponding fragment of St-*MC* cDNA was also used as a probe in DNA gel blots to identify transgenic *Arabidopsis* lines harboring single copies of *MPF3* or St-*MC*, respectively.

mRNA in Situ Hybridization

A 275-bp cDNA fragment spanning the C-domain and 3′-untranslated region of the *MPF3* cDNA was designed as probe template. Probes were synthesized using the T7 RNA polymerase driven by a T7 promoter and labeled with digoxigenin using the DIG-RNA labeling kit (Roche). Hybridization was performed as described by Carr and Irish (1997), except that the temperature for washing slides was 50°C in our experiments.

RT-PCR Analyses

Routine RT-PCR analysis was performed and PCR products were separated on a 1.2% agarose gel. Real-time RT-PCR was performed using the SYBR Premix Ex Taq (Perfect Real Time) kit (TaKaRa) on an Mx3000p real-time system (Stratagene) at an amplification cycle consisting of 30 s at 95°C for 1 cycle, followed by 40 cycles of 5 s at 95°C and 40 s at 60°C, which were followed by a dissociation curve. The *Actin* gene was used as the internal control.

Yeast Two-Hybrid Assays

The open reading frame (ORF) of *MPF3* was inserted into pGBKT7 and transformed into the yeast strain AH109 to check self-activation. MPF3 cannot self-activate, and the *MPF3* construct was transformed into Y187 as bait to screen the *Physalis* library. The medium, library information, and the procedures used were the same as described by He et al. (2007). The ORF of the MPF3-interacting partners was cloned into pGADT7. The cotransformed yeast cells with *MPF3* bait were grown on the selected plates SD/-His-Leu-Trp at 28°C for 5 d. Their interaction strength was determined by a galactosidase activity assay using *o*-nitrophenyl-β-D-galactoside as substrate according to the protocol of Clontech.

Pull-Down Assays

The ORF of *MPF3* was cloned into a pET-30a(+) vector containing a 6×His tag, expressed in *Escherichia coli* BL21 (DE3), and then purified on Ni Sepharose columns (GE Healthcare). ORFs of *PFGLO1* and *PFGLO2* were cloned into a pGEX-4T-1 vector with a glutathione *S*-transferase (GST) tag, expressed in *E. coli* BL21, and then loaded onto Glutathione Sepharose columns (GE Healthcare). The purified recombinant HIS-MPF3 proteins were loaded into the Glutathione Sepharose columns with GST-PFGLO1- and GST-PFGLO2-recombinant proteins, respectively, and incubated overnight at 4°C. The columns were then washed four times with binding buffer, and the bound proteins were eluted with washing buffer. The eluted proteins were heated and then separated on 12% SDS polyacrylamide gels. Proteins were blotted on nitrocellulose filter membranes by the semidry electrophoretic transfer method, and the membranes were blocked with 5% BSA-Tris-buffered saline containing 0.05% Tween-20 buffer for 1 h. Membranes were incubated with anti-GST or anti-HIS antibodies for 2 h and then with anti-horseradish peroxidase antibodies for 1 h. The membranes were washed with Tris-buffered saline containing 0.05% Tween-20 buffer three times after each incubation. Radioautographs of the filters were obtained using Kodak film at room temperature for 1 min and fixed according to standard procedures.

Subcellular Localization and BiFC

For subcellular localization, the ORF of *MPF3* was cloned into the Super1300 expression vector (Chen et al., 2009) using the *Xba*I-*Kpn*I cutting sites and fused to a GFP gene. For BiFC assays, the ORFs of *MPF3*, *MPF2*, *PFGLO1*, *PFGLO2*, and *PFAG* were cloned into a pair of vectors, pSPYNE-35S and pSPYCE-35S (Walter et al., 2004) through the *Xba*I and *Bam*HI cutting sites, respectively. The two vectors were designed to express either N- or C-terminal halves of a YFP. The recombinant MPF3-GFP construct or the construct combination of two proteins fused with the N- or C-terminal halves of YFP was injected into leaf epidermal cells of *Nicotiana benthamiana* via *Agrobacterium tumefaciens*. Forty-eight hours after injection, the GFP or YFP fluorescence signal was detected using confocal laser scanning microscopy (Olympus FV1000 MPE). The GFP signal intensity was quantified using ImageJ (http://rsb.info.nih.gov/nih-image; Abràmoff et al., 2004).

EMSA

The recombinant proteins HIS-MPF2, HIS-PFAG, GST-MPF3, GST-PFGLO1, and GST-PFGLO2 were expressed in *E. coli* and purified using Ni and Glutathione Sepharose columns (GE Healthcare). The EMSA was performed using the DIG gel-shift kit, 2nd generation (Roche). The 3′end labeling with digoxigenin-11-ddUTP double-stranded DNA probes was generated by annealing complementary oligonucleotides. The probe sequences are shown in Supplemental Table 3 online. The protein-DNA binding mixture was incubated at room temperature for 15 min and separated on a 6% native polyacrylamide gel. After blotting and cross-linking, the DIG-labeled probes were detected by chemiluminescence and then the membranes were exposed to x-ray film.

Plant Transformation and Genotyping Analysis

A 389-bp fragment of *MPF3* cDNA encoding partial K and full C domains and a partial 3′-untranslated region were inserted into the binary vector pFGC1008 (ChromDB; http://www.chromdb.org), resulting in a *MPF3*-RNAi construct. *MPF3* ORF cDNA was cloned into the plant binary vector pBin19 and overexpressed in *Physalis*. For transformation of *Arabidopsis*, the full-length cDNAs for *MPF3* and St-*MC* were inserted into pBAR. For *Physalis* transformation, the *Agrobacterium* strain LBA4404 was used. The medium and transformation procedures were identical to those described previously (He and Saedler, 2005). The GV3101 strain was used for transformation of *Arabidopsis* using the floral dip method (Clough and Bent, 1998). The transgenic *Physalis* plants were confirmed by real-time RT-PCR, and the transgenic *Arabidopsis* plants were confirmed by DNA gel blots.

VIGS Analyses

Three gene-silencing constructs were created to specifically downregulate *MPF2*, *MPF3*, or both. The fragments for *MPF2*-RNAi (He and Saedler, 2005) and for *MPF3*-RNAi were introduced either solely or tandemly into a TRV-mediated gene silencing system (Liu et al., 2002) and then applied to the leaves of 2-week-old *Physalis* seedlings. A 300-bp *PFPDS*-specific cDNA fragment was introduced into the TRV system as a control.

Morphological Analyses

For scanning electronic microscopy, fresh material was frozen in liquid nitrogen, sputter-coated with gold, and examined with a digital scanning microscope (Hitachi S-800). Cell and calyx size were quantified using the AxioVision LE image-processing program (http://www.zeiss.de). Calyces were taken from preanthesis flowers of the wild type and *MPF3*-RNAi lines indicated. Stamen sectioning was performed. Pollen maturation was

detected using I_2-KI staining. The main stem node number was recorded for flowering time in *Physalis*. The bolting time and rosette leaf number at the time of bolting were recorded to determine flowering time in *Arabidopsis*. For histological analyses, mature stamens were fixed in formalin-acetic acid-alcohol solution and dehydrated in a graded ethanol series. After replacing the ethanol with xylene, the stamens were embedded in paraffin wax (Sigma-Aldrich). Tissue sections were cut at 10 μm on a microtome and stained with safranine and fast green. All P values are based on two-tailed *t* tests.

Phylogenetic Reconstruction and Selection Evaluation

BLAST searches were performed in GenBank (http://www.ncbi.nlm.nih.gov/) using four *P. floridana AP1/SQUA*-like protein sequences as queries. The coding sequences were aligned and manually adjusted in BioEdit version 7.0.9 (Hall, 1999). The phylogeny was constructed based on the amino acid sequences, excluding the unalignable regions in the I and C domains, with MrBayes version 3.1.2 (Huelsenbeck and Ronquist, 2001) (prset aamodelpr = mixed; ngen =1000000), using two sequences from *Euptelea pleiosperma* as the outgroup. The maximum likelihood tree was also constructed using the PhyML v3.0 program (Guindon and Gascuel, 2003).

To determine whether there were changes in selection pressure among members of the *euAP1* clade, we used codon-based substitution models as implemented in PAML (Yang, 2007). The branch (model = 1; NSsites = 0; or model = 2; NSsites = 0) and branch-site models (model = 2; NSsites = 2) were performed (Yang, 1998; Zhang et al., 2005). Likelihood ratio tests were conducted using χ^2 tests to detect positive selection between each of the pairs of models (Nielsen and Yang, 1998).

Sequence Isolation

Total RNA was extracted from young floral buds with Plant RNA reagent (Invitrogen). First-strand cDNA was synthesized using SuperScript II reverse transcriptase (Invitrogen) with the poly(T) primer 5′-CCGGATCCTCTAGAGCGGCCG C(T)$_{17-30}$. The 3′ and 5′ ends of the *AP1/SQUA*-like cDNAs from *Physalis* were amplified according to the standard manual of the 3′/5′ RACE kit (Roche). The degenerate primers were 5′-AGNCAAGTNC-ANTTYTCAAAGAG-3′ and 5′-AARGGNAARATCTTTGARTAYTC-3′, and the adapter primer was 5′-CCGGATCCTCTAGAGCGGCCGC-3′. Full-length cDNA sequences were then obtained using gene-specific primers (see Supplemental Table 5 online). The orthologs of *MPF3* were previously isolated from *S. macrocarpon* (*MSM3*) and *S. tuberosum* (St-*MC*) with a routine RT-PCR (He et al., 2004).

All sequences were amplified using TaKaRa LA Taq polymerase. The amplified fragments were cloned into the pGEM-T Easy Vector (Promega), and the various expression constructs were commercially sequenced by Beijing Genomics Institute. The primer sequences used in this work are presented in Supplemental Table 5 online.

Accession Numbers

Sequence data from this article can be found in GenBank/EMBL databases under the following accession numbers: KC414859 (St-*MC*), KC414860 (*MSM3*), KC414861 (*PFFUL1*), KC414862 (*PFFUL2*), KC414863 (*PFFL*), KC414864 (*MPF3*), JX467691 (*PFGLO1*), KC174706 (*PFGLO2*) and KC794937 (*PFAG*).

Supplemental Data

The following materials are available in the online version of this article.

Supplemental Figure 1. Bayesian Interference of *AP1/SQUA*-Like Genes.

Supplemental Figure 2. Protein–Protein Dimerization among MPF3-Interacting Partners within the Yeast Two-Hybrid System.

Supplemental Figure 3. Anther Transverse Section Analyses.

Supplemental Figure 4. Expression of the Candidate Genes Involved in Sugar Partitioning Pathways.

Supplemental Figure 5. VIGS-Mediated *MPF3* Silencing Phenocopies *MPF3*-RNAi.

Supplemental Figure 6. Normal Pollen Development in the *35S:PDS*-VIGS Flowers.

Supplemental Figure 7. Cell Morphology in the Various ICSs.

Supplemental Figure 8. Functional Analyses in Transgenic *Arabidopsis*.

Supplemental Table 1. Variation in Flowering Time in Transgenic *Physalis* Plants.

Supplemental Table 2. MPF3 and MPF2 Modulate Cell Division and Cell Expansion during Calyx Development in *Physalis*.

Supplemental Table 3. Probe Sequences for EMSA.

Supplemental Table 4. Parameter Estimates under Branch and Branch-Site Models.

Supplemental Table 5. List of Primers Used in This Work.

Supplemental Data Set 1. Sequence Alignment of *AP1/SQUA*-Like Genes.

Supplemental Data Set 2. Sequence Information Used from the *Physalis* Floral Transcriptome.

AUTHOR CONTRIBUTIONS

C.H. designed the research project and conceived the experiments. J.Z., Y.T., S.R., and C.H. isolated sequences. Y.T. and J.Z. characterized expressions with real-time RT-PCR. Y.T. and J.Z. performed overexpression and RNAi analyses. J.S.Z. conducted mRNA in situ hybridization. J.Z. and P.G. searched *Physalis* genes involved in sugar partitioning pathways. J.S.Z., P.G., and J.Z. performed relative quantification of protein–protein interaction strength in yeast. J.S.Z. performed pulldowns. R.S. performed yeast library screens. C.H. and S.R. performed transgenic *Arabidopsis* analyses. J.Z. conducted other experiments. M.Z. and Y.T. performed evolution analyses. C.H. and J.Z. analyzed the data. C.H. wrote the article.

REFERENCES

Abràmoff, M.D., Magalhães, P.J., and Ram, S.J. (2004). Image processing with ImageJ. Biophotonics Int. **11:** 36–42.

Ampomah-Dwamena, C., Morris, B.A., Sutherland, P., Veit, B., and Yao, J.L. (2002). Down-regulation of *TM29*, a tomato *SEPALLATA* homolog, causes parthenocarpic fruit development and floral reversion. Plant Physiol. **130:** 605–617.

Becker, A., and Theissen, G. (2003). The major clades of MADS-box genes and their role in the development and evolution of flowering plants. Mol. Phylogenet. Evol. **29:** 464–489.

Benlloch, R., d'Erfurth, I., Ferrandiz, C., Cosson, V., Beltrán, J.P., Cañas, L.A., Kondorosi, A., Madueño, F., and Ratet, P. (2006). Isolation of *mtpim* proves *Tnt1* a useful reverse genetics tool in *Medicago truncatula* and uncovers new aspects of *AP1*-like functions in legumes. Plant Physiol. **142:** 972–983.

Berbel, A., Navarro, C., Ferrándiz, C., Cañas, L.A., Madueño, F., and Beltrán, J.P. (2001). Analysis of *PEAM4*, the pea *AP1* functional homologue, supports a model for *AP1*-like genes controlling both floral meristem and floral organ identity in different plant species. Plant J. **25:** 441–451.

Bowman, J.L., Alvarez, J., Weigel, D., Meyerowitz, E.M., and Smyth, D.R. (1993). Control of flower development in *Arabidopsis thaliana* by *APETALA1* and interacting genes. Development **119:** 721–743.

Büttner, M. (2007). The monosaccharide transporter(-like) gene family in *Arabidopsis*. FEBS Lett. **581:** 2318–2324.

Carr, S.M., and Irish, V.F. (1997). Floral homeotic gene expression defines developmental arrest stages in *Brassica oleracea* L. vars. *botrytis* and *italica*. Planta **201:** 179–188.

Chen, Y.F., Li, L.Q., Xu, Q., Kong, Y.H., Wang, H., and Wu, W.H. (2009). The WRKY6 transcription factor modulates *PHOSPHATE1* expression in response to low Pi stress in *Arabidopsis*. Plant Cell **21:** 3554–3566.

Clough, S.J., and Bent, A.F. (1998). Floral dip: A simplified method for *Agrobacterium*-mediated transformation of *Arabidopsis thaliana*. Plant J. **16:** 735–743.

Coen, E.S., and Meyerowitz, E.M. (1991). The war of the whorls: Genetic interactions controlling flower development. Nature **353:** 31–37.

Davies, B., Egea-Cortines, M., de Andrade Silva, E., Saedler, H., and Sommer, H. (1996). Multiple interactions amongst floral homeotic MADS box proteins. EMBO J. **15:** 4330–4343.

Davies, B., Motte, P., Keck, E., Saedler, H., Sommer, H., and Schwarz-Sommer, Z. (1999). PLENA and FARINELLI: Redundancy and regulatory interactions between two *Antirrhinum* MADS-box factors controlling flower development. EMBO J. **18:** 4023–4034.

de Folter, S., Immink, R.G.H., Kieffer, M., Parenicová, L., Henz, S.R., Weigel, D., Busscher, M., Kooiker, M., Colombo, L., Kater, M.M., Davies, B., and Angenent, G.C. (2005). Comprehensive interaction map of the *Arabidopsis* MADS box transcription factors. Plant Cell **17:** 1424–1433.

Ditta, G., Pinyopich, A., Robles, P., Pelaz, S., and Yanofsky, M.F. (2004). The *SEP4* gene of *Arabidopsis thaliana* functions in floral organ and meristem identity. Curr. Biol. **14:** 1935–1940.

Egea-Cortines, M., Saedler, H., and Sommer, H. (1999). Ternary complex formation between the MADS-box proteins SQUAMOSA, DEFICIENS and GLOBOSA is involved in the control of floral architecture in *Antirrhinum majus*. EMBO J. **18:** 5370–5379.

Ferrándiz, C., Gu, Q., Martienssen, R., and Yanofsky, M.F. (2000). Redundant regulation of meristem identity and plant architecture by *FRUITFULL*, *APETALA1* and *CAULIFLOWER*. Development **127:** 725–734.

Gregis, V., Sessa, A., Dorca-Fornell, C., and Kater, M.M. (2009). The *Arabidopsis* floral meristem identity genes *AP1*, *AGL24* and *SVP* directly repress class B and C floral homeotic genes. Plant J. **60:** 626–637.

Guindon, S., and Gascuel, O. (2003). A simple, fast, and accurate algorithm to estimate large phylogenies by maximum likelihood. Syst. Biol. **52:** 696–704.

Gustafson-Brown, C., Savidge, B., and Yanofsky, M.F. (1994). Regulation of the *Arabidopsis* floral homeotic gene *APETALA1*. Cell **76:** 131–143.

Hall, T.A. (1999). BioEdit: A user-friendly biological sequence alignment editor and analysis program for Windows 95/98/NT. Nucleic Acids Symp. Ser. **41:** 95–98.

He, C.Y., Münster, T., and Saedler, H. (2004). On the origin of floral morphological novelties. FEBS Lett. **567:** 147–151.

He, C.Y., and Saedler, H. (2005). Heterotopic expression of *MPF2* is the key to the evolution of the Chinese lantern of *Physalis*, a morphological novelty in Solanaceae. Proc. Natl. Acad. Sci. USA **102:** 5779–5784.

He, C.Y., and Saedler, H. (2007). Hormonal control of the inflated calyx syndrome, a morphological novelty, in *Physalis*. Plant J. **49:** 935–946.

He, C.Y., Sommer, H., Grosardt, B., Huijser, P., and Saedler, H. (2007). PFMAGO, a MAGO NASHI-like factor, interacts with the MADS-domain protein MPF2 from *Physalis floridana*. Mol. Biol. Evol. **24:** 1229–1241.

He, C.Y., Zhang, J.S., and Chen, S.Y. (2002). A soybean gene encoding a proline-rich protein is regulated by salicylic acid, an endogenous circadian rhythm and by various stresses. Theor. Appl. Genet. **104:** 1125–1131.

Honma, T., and Goto, K. (2001). Complexes of MADS-box proteins are sufficient to convert leaves into floral organs. Nature **409:** 525–529.

Hu, J.Y., and Saedler, H. (2007). Evolution of the inflated calyx syndrome in Solanaceae. Mol. Biol. Evol. **24:** 2443–2453.

Huelsenbeck, J.P., and Ronquist, F. (2001). MRBAYES: Bayesian inference of phylogenetic trees. Bioinformatics **17:** 754–755.

Huijser, P., Klein, J., Lönnig, W.E., Meijer, H., Saedler, H., and Sommer, H. (1992). *Bracteomania*, an inflorescence anomaly, is caused by the loss of function of the MADS-box gene *squamosa* in *Antirrhinum majus*. EMBO J. **11:** 1239–1249.

Immink, R.G.H., Kaufmann, K., and Angenent, G.C. (2010). The 'ABC' of MADS domain protein behaviour and interactions. Semin. Cell Dev. Biol. **21:** 87–93.

Kanno, A., Saeki, H., Kameya, T., Saedler, H., and Theissen, G. (2003). Heterotopic expression of class B floral homeotic genes supports a modified ABC model for tulip (*Tulipa gesneriana*). Plant Mol. Biol. **52:** 831–841.

Kaufmann, K., Wellmer, F., Muiño, J.M., Ferrier, T., Wuest, S.E., Kumar, V., Serrano-Mislata, A., Madueño, F., Krajewski, P., Meyerowitz, E.M., Angenent, G.C., and Riechmann, J.L. (2010). Orchestration of floral initiation by APETALA1. Science **328:** 85–89.

Khan, M.R., Hu, J., and Ali, G.M. (2012). Reciprocal loss of CArG-boxes and auxin response elements drives expression divergence of *MPF2-Like* MADS-box genes controlling calyx inflation. PLoS ONE **7:** e42781.

Leggewie, G., Kolbe, A., Lemoine, R., Roessner, U., Lytovchenko, A., Zuther, E., Kehr, J., Frommer, W.B., Riesmeier, J.W., Willmitzer, L., and Fernie, A.R. (2003). Overexpression of the sucrose transporter SoSUT1 in potato results in alterations in leaf carbon partitioning and in tuber metabolism but has little impact on tuber morphology. Planta **217:** 158–167.

Leseberg, C.H., Eissler, C.L., Wang, X., Johns, M.A., Duvall, M.R., and Mao, L. (2008). Interaction study of MADS-domain proteins in tomato. J. Exp. Bot. **59:** 2253–2265.

Litt, A. (2007). An evaluation of A-function: Evidence from the *APETALA1* and *APETALA2* gene lineages. Int. J. Plant Sci. **168:** 73–91.

Litt, A., and Irish, V.F. (2003). Duplication and diversification in the *APETALA1/FRUITFULL* floral homeotic gene lineage: Implications for the evolution of floral development. Genetics **165:** 821–833.

Litt, A., and Kramer, E.M. (2010). The ABC model and the diversification of floral organ identity. Semin. Cell Dev. Biol. **21:** 129–137.

Liu, Y., Schiff, M., and Dinesh-Kumar, S.P. (2002). Virus-induced gene silencing in tomato. Plant J. **31:** 777–786.

Mandel, M.A., Gustafson-Brown, C., Savidge, B., and Yanofsky, M.F. (1992). Molecular characterization of the *Arabidopsis* floral homeotic gene *APETALA1*. Nature **360:** 273–277.

Mandel, M.A., and Yanofsky, M.F. (1995). A gene triggering flower formation in *Arabidopsis*. Nature **377:** 522–524.

Ng, M., and Yanofsky, M.F. (2001). Activation of the *Arabidopsis* B class homeotic genes by *APETALA1*. Plant Cell **13:** 739–753.

Nielsen, R., and Yang, Z. (1998). Likelihood models for detecting positively selected amino acid sites and applications to the HIV-1 envelope gene. Genetics **148:** 929–936.

Oliver, S.N., Van Dongen, J.T., Alfred, S.C., Mamun, E.A., Zhao, X., Saini, H.S., Fernandes, S.F., Blanchard, C.L., Sutton, B.G., Geigenberger, P., Dennis, E.S., and Dolferus, R. (2005). Cold-induced repression of the rice anther-specific cell wall invertase gene *OSINV4* is correlated with sucrose accumulation and pollen sterility. Plant Cell Environ. **28:** 1534–1551.

Pabón-Mora, N., Ambrose, B.A., and Litt, A. (2012). Poppy *APETALA1/FRUITFULL* orthologs control flowering time, branching, perianth identity, and fruit development. Plant Physiol. **158:** 1685–1704.

Pelaz, S., Ditta, G.S., Baumann, E., Wisman, E., and Yanofsky, M.F. (2000). B and C floral organ identity functions require *SEPALLATA* MADS-box genes. Nature **405:** 200–203.

Peña, L., Martín-Trillo, M., Juárez, J., Pina, J.A., Navarro, L., and Martínez-Zapater, J.M. (2001). Constitutive expression of *Arabidopsis LEAFY* or *APETALA1* genes in citrus reduces their generation time. Nat. Biotechnol. **19:** 263–267.

Preston, J.C., and Kellogg, E.A. (2006). Reconstructing the evolutionary history of paralogous *APETALA1/FRUITFULL*-like genes in grasses (Poaceae). Genetics **174:** 421–437.

Ranwala, A.P., and Miller, W.B. (1998). Sucrose-cleaving enzymes and carbohydrate pools in *Lilium longiflorum* floral organs. Physiol. Plant. **103:** 541–550.

Riß, S. (2009). Isolation and Analysis of *MPF2*-Like MADS-Box Genes from Physaleae and Characterization of Their *cis*-Regulatory Regions. PhD dissertation (Koeln, Germany: Universität zu Köln).

Schwarz-Sommer, Z., Huijser, P., Nacken, W., Saedler, H., and Sommer, H. (1990). Genetic control of flower development by homeotic genes in *Antirrhinum majus*. Science **250:** 931–936.

Shan, H.Y., Zhang, N., Liu, C.J., Xu, G.X., Zhang, J., Chen, Z.D., and Kong, H.Z. (2007). Patterns of gene duplication and functional diversification during the evolution of the *AP1/SQUA* subfamily of plant MADS-box genes. Mol. Phylogenet. Evol. **44:** 26–41.

Taylor, S.A., Hofer, J.M.I., Murfet, I.C., Sollinger, J.D., Singer, S.R., Knox, M.R., and Ellis, T.H. (2002). *PROLIFERATING INFLORESCENCE MERISTEM*, a MADS-box gene that regulates floral meristem identity in pea. Plant Physiol. **129:** 1150–1159.

Theissen, G., and Melzer, R. (2007). Molecular mechanisms underlying origin and diversification of the angiosperm flower. Ann. Bot. (Lond.) **100:** 603–619.

Theissen, G., and Saedler, H. (2001). Plant biology. Floral quartets. Nature **409:** 469–471.

Tröbner, W., Ramirez, L., Motte, P., Hue, I., Huijser, P., Lönnig, W. E., Saedler, H., Sommer, H., and Schwarz-Sommer, Z. (1992). *GLOBOSA*: A homeotic gene which interacts with DEFICIENS in the control of *Antirrhinum* floral organogenesis. EMBO J. **11:** 4693–4704.

Urbanus, S.L., de Folter, S., Shchennikova, A.V., Kaufmann, K., Immink, R.G.H., and Angenent, G.C. (2009). *In planta* localisation patterns of MADS domain proteins during floral development in *Arabidopsis thaliana*. BMC Plant Biol. **9:** 5.

Urbanus, S.L., Martinelli, A.P., Dinh, Q.D., Aizza, L.C., Dornelas, M.C., Angenent, G.C., and Immink, R.G.H. (2010). Intercellular transport of epidermis-expressed MADS domain transcription factors and their effect on plant morphology and floral transition. Plant J. **63:** 60–72.

Vrebalov, J., Ruezinsky, D., Padmanabhan, V., White, R., Medrano, D., Drake, R., Schuch, W., and Giovannoni, J. (2002). A MADS-box gene necessary for fruit ripening at the tomato *ripening-inhibitor* (*rin*) locus. Science **296:** 343–346.

Walter, M., Chaban, C., Schütze, K., Batistic, O., Weckermann, K., Näke, C., Blazevic, D., Grefen, C., Schumacher, K., Oecking, C., Harter, K., and Kudla, J. (2004). Visualization of protein interactions in living plant cells using bimolecular fluorescence complementation. Plant J. **40:** 428–438.

Weigel, D., and Meyerowitz, E.M. (1994). The ABCs of floral homeotic genes. Cell **78:** 203–209.

West, A.G., Shore, P., and Sharrocks, A.D. (1997). DNA binding by MADS-box transcription factors: A molecular mechanism for differential DNA bending. Mol. Cell. Biol. **17:** 2876–2887.

Wu, X., Dinneny, J.R., Crawford, K.M., Rhee, Y., Citovsky, V., Zambryski, P.C., and Weigel, D. (2003). Modes of intercellular transcription factor movement in the *Arabidopsis* apex. Development **130:** 3735–3745.

Yang, Z.H. (1998). Likelihood ratio tests for detecting positive selection and application to primate lysozyme evolution. Mol. Biol. Evol. **15:** 568–573.

Yang, Z.H. (2007). PAML 4: Phylogenetic analysis by maximum likelihood. Mol. Biol. Evol. **24:** 1586–1591.

Yu, H., Ito, T., Wellmer, F., and Meyerowitz, E.M. (2004). Repression of *AGAMOUS-LIKE* 24 is a crucial step in promoting flower development. Nat. Genet. **36:** 157–161.

Zhang, H., Liang, W.Q., Yang, X.J., Luo, X., Jiang, N., Ma, H., and Zhang, D.B. (2010). *Carbon starved anther* encodes a MYB domain protein that regulates sugar partitioning required for rice pollen development. Plant Cell **22:** 672–689.

Zhang, J.S., Khan, M.R., Tian, Y., Li, Z.C., Riss, S., and He, C.Y. (2012). Divergences of MPF2-like MADS-domain proteins have an association with the evolution of the inflated Calyx syndrome within Solanaceae. Planta **236:** 1247–1260.

Zhang, J.Z., Nielsen, R., and Yang, Z.H. (2005). Evaluation of an improved branch-site likelihood method for detecting positive selection at the molecular level. Mol. Biol. Evol. **22:** 2472–2479.